Politecnico di Torino

Renewable Energy Systems
A.Y. 2022/2023
March 2023

Techno-Economic Evaluation of Alkaline Electrolyzers for Green H_2 Production from Seawater

Advisors:

Andrea Lanzini
Rafael D'Amore Domenech

Candidate:

Francesco Currenti

Summary

List of figures

List of tables

Abstract

This thesis aims to investigate the topic of green hydrogen production through the electrolysis reaction from desalinated saltwater to analyze the current technical and economic issues.

First, a general overview of the electrolyzers currently available on the market and under development is given, which reveals that the best option for hydrogen production at sea are alkaline electrolyzers, as they represent the cheapest and most efficient technology in this field. Furthermore, it is shown that it is possible to produce the electrolyte on-site through the Chloralkali process, avoiding the risks and costs of its manual replacement.

Then, the advantages and disadvantages of hydrogen production at sea are highlighted, pointing out that the use of saltwater for hydrogen production will be crucial in the future to avoid problems of freshwater scarcity and environmental impact. For this reason, all water purification techniques are analyzed, detailing the advantages and disadvantages of each technology.

In parallel to the theoretical analysis, an experimental part is carried out in which a synthetic seawater mixture is prepared and distilled to evaluate the salt rejection rate following a serial distillation. Chromatography results show that a single distillation is the right compromise between residual salinity and cost, and that only a more efficient process, such as electrodialysis, can further reduce the salinity level after the first distillation.

From these results, a saltwater solution with the salinity values related to the first distillation is created and mixed with different quantity of distilled water to simulate the operation of the electrolyzer at different times.

In the meantime, various trials and errors are carried out before the functional alkaline electrolyzer could be printed in the correct way with the 3D printer. The cell is initially printed entirely with *PLA*, but with poor results as this material is not very resistant to caustic soda and high temperatures. Then the cell is designed and printed with polypropylene, using PLA as the support structure, and the results are much better due to the better physical and chemical properties of this material.

Once obtained the functional cell, it is connected to the entire system in the test bench to produce hydrogen and evaluate the voltage increase over time due to the degradation of the electrolyte. The results obtained reveal for the first time in the available literature that the degradation of the electrolyte follows a reasonably accurate logarithmic pattern, which allows to calculate the electrolyte renewable time and its management cost at sea.

In contrast to all previous analyses, these results show that the electrolyte must be changed only 5 times during the entire life cycle of the electrolyzer to maintain high efficiency. From this analysis, it can be also noticed that the additional cost of the electrolyte management cost, calculated for the first time in the available literature in line with what it is currently available in the market, is not excessively high with respect to the levelized cost of hydrogen of the case study production plant (6.35 €/kg).

The electrolyte management cost results in fact equal to 0.12 €/kg in the worst-case scenario and represents the 8% of the total plant costs, and a percentage lower than 2% with respect to the total levelized cost of hydrogen. Nevertheless, further innovations in the technology can further lower costs by making seawater electrolysis even more commercially competitive.

1. Introduction

1.1. Motivation

Climate change is one of the most difficult and urgent global challenges facing the world today. The major cause of global warming has been human activity which, since the beginning of the 19th century has started to use fossil fuels in industry, transportation, residential and commercial sectors.

In recent years, climate change has been exacerbated and amplified by an increase in global energy demand and consumption due to rapid population growth, which reached 8 billion in 2022, and an increase in economic prosperity. In Figure 1, it is possible to see that, over the past twenty-five years, the trend was only reversed during the financial-economic and health crises, which occurred in 2008 and 2020, respectively.

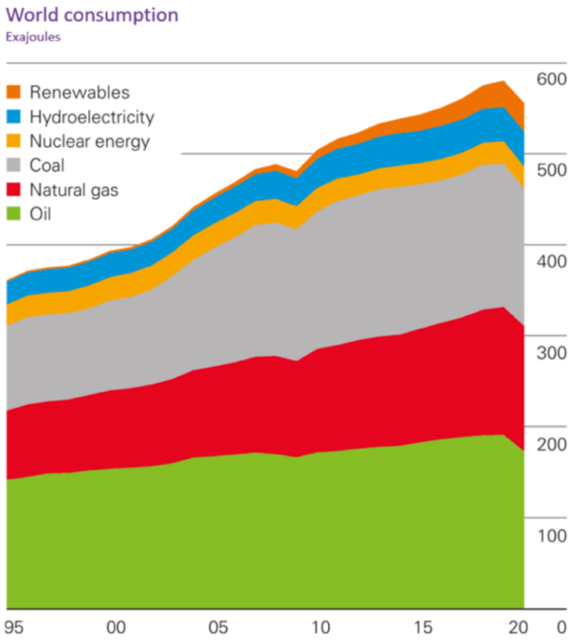

Figure 1: World energy consumption trend (Arias L.A., 2018)

Nowadays, most energy demand is still met using fossil fuels like coal, natural gas, and oil, that are characterized by high greenhouse gas emissions (CO_2, CH_4, N_2O and fluorinated gases) into the atmosphere (Arias L.A., 2018). These gases are extremely dangerous for the planet because they trap heat radiated from the Earth's surface causing the planet's temperature to rise and the increase in extreme weather phenomena such as flooding, glacier meltdown, increase of the sea level, species extinction, catastrophic storms, fires, etc.

To mitigate global warming and safeguard the planet, 196 countries and international organizations signed the *Paris Climate Agreement* in 2015. The goals of this international treaty are very ambitious and have the main objective of limiting the temperature increase to 1.5° with respect to the pre-industrial levels (United Nations Climate Change, 2023). The achievement of this goal is closely related to both increased energy efficiency of industrial processes and buildings and increased energy production from renewable sources, such as solar and photovoltaic, wind, and marine energy.

For this reason, the past few years have been characterized by an increase in subsidies and incentives for renewable energy resources, resulting in an increase in overall demand and a consequent sharp decrease in costs, as can be seen in Figure 2. In addition, the Figure 3 shows how the rising costs of fossil fuels in 2021 and 2022 have accelerated the competitiveness of renewables in the market.

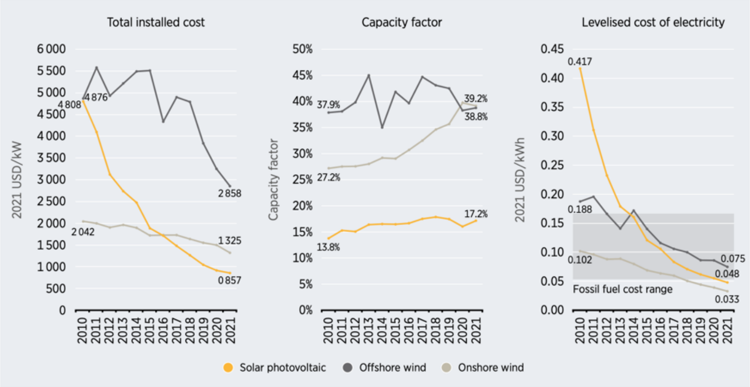

Figure 2: Renewable costs trend (IRENA, 2022)

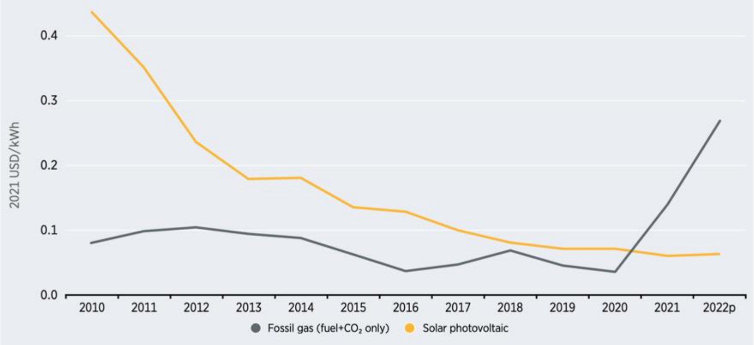

Figure 3: Comparison between solar photovoltaic and fossil fuel prices (IRENA, 2022)

Among renewable energy sources, two categories can be distinguished based on the placement of the plant: devices located on land are called *onshore*, while those located at sea are known as *offshore*. Despite the increased complexity in construction and maintenance, the interest on offshore renewables have increased a lot during the last years because they present many advantages over onshore technologies.

Firstly, offshore devices can exploit higher resources while having only minimal impact on the marine ecosystem and reducing both visual impact and noise levels near cities. Moreover, the large amount of free space available in the sea allows the design and installation of larger structures to collect more energy than onshore devices (Euronews, 2020).

Both onshore and offshore renewables can play a key role in decarbonizing hydrogen production, which nowadays comes mostly from highly polluting processes such as steam methane reforming, partial oxidation of heavy hydrocarbons and coal gasification. Renewable sources can in fact be coupled to electrolyzers to provide them with the electricity needed to produce green hydrogen through the water electrolysis process.

Water electrolysis is a non-spontaneous reaction that involves the breaking down of the water molecule H_2O into its elementary components (H_2, O_2) when the electrolyzer is powered by electricity coming from a direct current power source.

$$H_2O \rightarrow H_2 + \frac{1}{2}O_2 \quad \Delta G > 0 \quad (1)$$

Water electrolysis was discovered by a German physicist called *J.W. Ritter* and, although this technology has existed for over 200 years, today hydrogen production accounts for only 4% of the total.

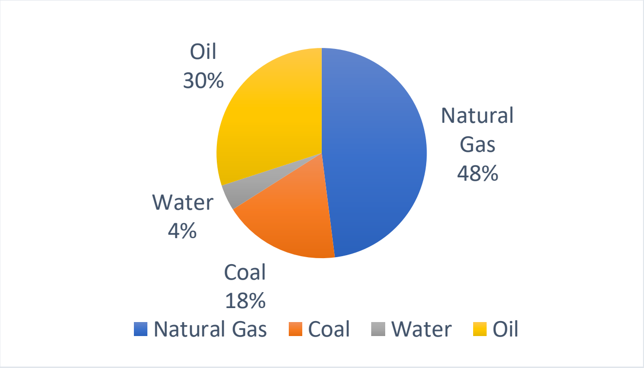

Figure 4: Hydrogen production methods share (Voldsund M., 2016)

Currently, hydrogen comes exclusively from freshwater, a precious and finite resource whose depletion would cause both availability problems for human activities and the ecosystem, as well as not insignificant environmental impacts.

Nevertheless, it is possible to produce hydrogen from a significantly more abundant resource on Earth: *Saltwater*. Saltwater electrolysis is still a developing technology because it presents technical and economic issues regarding possible salt damage to electrodes and the electrolyte.

The high-purity hydrogen produced by this reaction can be used as a fuel for internal combustion engines or hydrogen-powered vehicles, as a chemical reagent to produce fertilizers or other chemicals, and for oil refining.

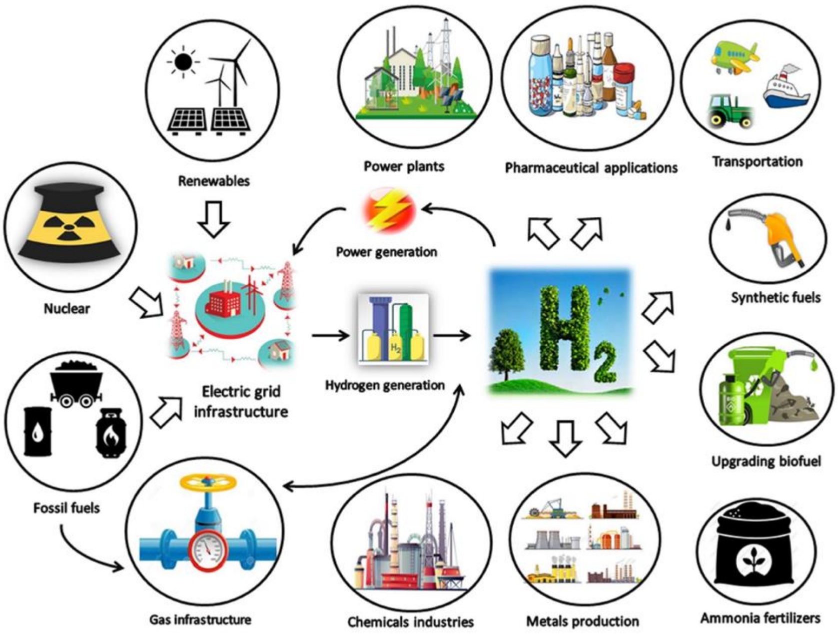

Figure 5: Hydrogen production and uses (Osman A.I., 2021)

In addition, hydrogen represents the most promising chemical energy storage medium due to its high capacity to store large amounts of energy in a compact and easily transportable form. Despite hydrogen is characterized by low energy density by volume in comparison with fossil fuels at normal conditions, the energy density of hydrogen can be increased by compression, liquefaction or by involving chemical reactions (Meng, 2006).

Compressed hydrogen is usually stored in high-pressure tanks, geological storage or other underground technologies and its energetic density increases with increasing pressure (Elberry A.M., 2021). On the other hand, *liquid hydrogen* achieves even higher energy density values but has technical and economic constraints because it requires a cryogenic cycle to maintain the liquefaction temperature (20.22 K, 1 bar). In addition to this, extreme insulation from the environment is required to prevent the hydrogen evaporation (Osman A.I., 2021).

The use of hydrogen as an energy storage medium represents a possible solution to the high degree of variability in the production of renewable sources due to the close dependence on atmospheric factors such as wind and solar irradiation. More specifically, hydrogen allows energy produced from renewable sources to be stored when production is greater than demand and then converted back into electricity using fuel cells during periods of low production. (Lucia, 2014)

Fuel cells are governed by the following spontaneous reaction:

$$H_2 + \frac{1}{2}O_2 \rightarrow H_2O \qquad \Delta G < 0 \quad (2)$$

1.2. Electrolyzers fundamentals

Electrolyzers are electrochemical cells capable of transforming electrical energy into chemical energy through a complete redox reaction separated into two different steps. They consist of two electrodes with opposite polarities: the negative pole is called *cathode* and hosts the reduction reaction, while the positive pole, the *anode,* is characterized by the *oxidation reaction* and the delivering of electrons (Treccani, 2023).

$$Cathode\ reaction\colon 2H^{+} + 2e^{-} \rightarrow H_2 \quad (3)$$

$$Anode\ reaction\colon H_2O \rightarrow \frac{1}{2}O_2 + 2H^{+} + 2e^{-} \quad (4)$$

The electrons released from the anode pass through the outer circuit before reaching the cathode where recombination takes place. In addition to the electron exchange, the electrolyzers are characterized by *ion exchange* through the electrolyte. Positive ions travel from the anode to the cathode, while negative ions take the opposite path.

Electrodes are usually coated with *catalysts,* namely materials added to the process that participate in the reaction remaining unchanged. The catalysts can host the reactants by absorption in its sites generating a structure with a different energy level called activated complex. The main role of these materials is to modify the energy pathway of the reaction improving the reaction speed and guaranteeing a better kinetics (Treccani, 2023).

Between the electrodes there is the *electrolyte,* a substance that undergoes the subdivision of its molecules into ions with good mobility in solution. The electrolyte must ensure good ion conduction, extremely low electron conduction and low molecular gas diffusion. Both oxidation and reduction reaction generate a *charge separation* that generates voltage gradients at the anode and at the cathode, whose difference is called *voltage gradient across the cell* and is defined as:

$$E_c = E_0 \pm \frac{RT}{nF} ln\left(\frac{[X^{+}]^{c}[Y^{-}]^{d}}{[X]^{a}[Y]^{b}}\right) \qquad (5)$$

Where E_0 is the *Nernst voltage*, R is the *ideal gas constant*, F is the *Faraday constant,* T is the temperature, n is the *stoichiometric number of moles of the transferred electrons*, X and Y represent the *concentration of the redox reactants*, the exponents are the stoichiometric coefficients of the reaction. (Tan S.Y., 2020). The equation above can be also written as:

$$E_c = E_0 \pm (\eta_{act} + \eta_{ohm} + \eta_{conc}) \quad (6)$$

Where and η_{act}, η_{ohm} ,η_{conc} represent respectively the *activation, ohmic* and *diffusion or concentration overvoltage.* The sign of the parenthesis depends on the *Gibbs free energy (ΔG):* if this quantity is negative the sign is minus, while in the opposite case the sign is plus.

The Nernst voltage is also called *open circuit voltage (OCV)* or *reversible voltage,* and it represents the voltage gradient between the electrodes in equilibrium. By the time that the equilibrium is broken closing the circuit, transport phenomena such as *charge transfer, charge migration* and *transport* happen. The charge transfer is due to the kinetic of electrochemical reactions at the electrodes and cause a drop of voltage called activation overvoltage. This represents the potential difference that is needed to overcome the activation energy of the reaction and generate a given current. The charge migration concerns a voltage drop called ohmic overvoltage due to the resistances of the different components that hinder ion migration in electrolyte and the electrons conduction both in the electrodes and the external circuit. Finally, the *concentration or diffusion overvoltage* is caused by the mass transport due to the molecular diffusion inside the electrodes. (Wang W., 2015)

The *polarization curve* in Figure 6 shows the kinetic behavior of different electrolyzers, highlighting the variation of the cell voltage as the current density. In these devices the increase in cell voltage is a clearly negative factor because, being a forced reaction, implies an increase in the work that must be provided to make the reaction take place. On the contrary, the increase in temperature is a positive factor as it allows the voltage to be lowered for the same current density. Higher temperatures consequently guarantee both a reduction in consumption and an improvement in electrolyzer performance.

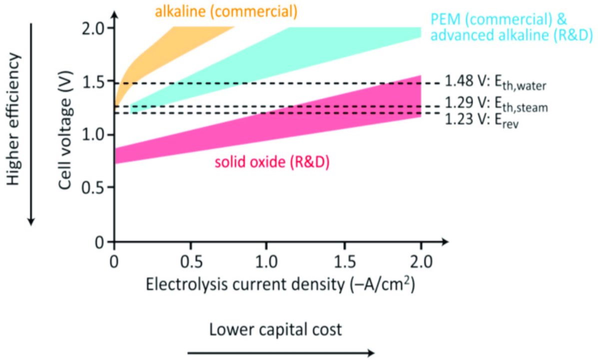

Figure 6: Polarization curve for the different electrolyzers (Barelli L., 2017)

1.3. Objectives

The main objective of this experimental thesis is the study of the technical and economic feasibility of the green hydrogen production with an electrolyzer from seawater.
To achieve our goal, it was necessary to:

- Select the most suitable type of electrolyzer for use with desalinated salt water.
- Investigate different water desalination technologies and experimentally evaluate the rejection rate between distillations to choose the most appropriate number of distillations in series for use in electrolyzers.
- Find a suitable distillation at low salt levels to increase the purity of water before entering the electrolyzer.
- Find a suitable material for printing a functional alkaline cell with the lab's 3D printer.
- Evaluate polarization curves at different operating times to estimate the electrolyte performance degradation trend.
- Assess the renewal time and the additional cost of the electrolyte compared to the total cost of the hydrogen production plant.

1.4. Thesis structure

This experimental thesis has been divided into six chapters:

1. *Introduction*: This chapter explains the reasons for the choice of the research topic, considering the current historical and social situation, and highlights the objectives of the experimental part.

2. *State of the Art*: This chapter classifies the most promising technologies currently on the market and the ones under development, pointing out similarities and differences between them.

3. *Hydrogen production from Seawater*: This chapter defines a reference seawater so that experiments can be reproduced and introduces the main topic of our thesis, the production of hydrogen at sea, pointing out the importance of the Chloralkali reaction for the electrolyte production on-site. This chapter also describes the various technologies for desalinating salt water.

4. *Materials and Methods:* This chapter provides a description of the materials, design, and assembly of the cell. Furthermore, this chapter aims to show all the methodology used to obtain the laboratory and case study results.

5. *Results and Discussion*: This chapter shows all the results obtained in the laboratory concerning the salinity change after various series distillations and the polarization curves at different operating times, as well as the results of the economic evaluation of the case study

6. *Conclusions*: This chapter summarizes the results obtained from the theoretical analysis, the case study and laboratory experiments.

2. State of the art

Electrolyzers can be classified according to several factors, such as temperature, configuration, or scale of hydrogen production. However, the most popular subdivision for differentiating electrolyzers concerns the type of electrolyte used.

The electrolyzers currently on the market are:

- *Alkaline Water Electrolyzers (AWE)*

- *Polymer Electrolyte Membrane Electrolyzers (PEM)*

On the other hand, the electrolyzers still in the research and study phase are:

- *Solid Oxide Electrolyzers (SOE)*

- *Alkaline Anion Exchange Membranes Electrolyzers (AEM)*

2.1. Alkaline Water Electrolyzers (AWE)

Alkaline water electrolysis is the first technology to enter the market and the simplest for producing hydrogen. *AWEs* represent a commercially mature technology, characterized by a temperature operating range between 70 and 90 °C (Shiva Kumar S., 2022), and pressure levels below 30 bar (Brauns J., 2020).

These devices are characterized by limited current density and safety issues due to the use of a corrosive electrolyte. Nevertheless, the *AWEs* have long-term stability and represent the least expensive alternative as they do not require precious catalysts such as noble metals (Shiva Kumar S., 2022).

The electrodes of an alkaline water electrolyzer are composed of metal materials. The cathode can be made of metals with high overpotentials (Cd, Ti, Zn, etc.), medium overpotentials (Fe, Co, Ni, Cu, etc.) and low overpotentials (Pt, Pd). On the other hand, the most employed material for the anode is nickel, although cathode materials can also be used (Rashid M.M., 2015).

Both electrodes are covered with transition metal-based catalysts to accelerate the reaction rate by lowering the activation energy and to avoid high overvoltage in both the oxidation and reduction reactions. More specifically, the kinetics of the reaction is improved through the addition of cobalt or molybdenum, galvanic deposition of Ni-Zn, Ni-Co-Zn alloys on the electrode support, or by vacuum plasma spraying (Rashid M.M., 2015).

The most used electrolyte for alkaline water electrolysis is liquid KOH at high concentrations ranging from 20 to 40% (López-Fernández E., 2021), because it presents an optimal specific conductivity in the operating temperature range at these concentrations.

Other electrolytes used for the Alkaline electrolyzer are NaOH solutions, which are less expensive and makes it easier to produce hydrogen at sea as caustic soda can be produced through the Chloralkali reaction. Sodium hydroxide solutions are also characterized by lower solubility of the product gas than potassium hydroxide because they exhibit a lower salting-out effect (Brauns J., 2020). This represents a clear drawback of the KOH solutions because this phenomenon causes a steep increase of the losses and a decrease of the purity of the gas produced.

In addition, another problem of this electrolyte is its high sensitivity to CO_2 of the environment that causes the production of K_2CO_3, whose precipitation can cause the clogging of the pores of the anode gas diffusion layer and lower the ionic conductivity of the electrolyte (López-Fernández E., 2021).

However, KOH solutions are characterized by higher ionic conductivity than the NaOH ones. More specifically, at the optimal weight percentage, the KOH conductivity is 40-50% higher than the one of NaOH.

Ionic liquids (ILs) can also represent an alternative as electrolytes thanks to their remarkable properties such as negligible vapor pressure, thermal stability, non-inflammability, and chemical inertia. They are organic substances characterized by a great electrical conduction and by the fact that they are liquid at room temperature. They provide a very good efficiency at low temperatures and do not require expensive electrodes materials, but their use is constrained by the high viscosity and the low information about their toxicity (Brauns J., 2020).

All these electrolytes' solutions are highly corrosive, and an addition of other materials is needed to prevent a decrease in catalytic activity and avoid damages to the electrodes with a consequent increase in operating costs.

Between the two electrodes of an *AWE* there is the *diaphragm*, a thin and porous foil with a thickness between 0.05 and 0.5 millimeters able to transport the hydroxide ions OH^- and avoid the gas cross-over to prevent the recombination (Miller H.A., 2020). This component also avoids the formation of unwanted water at the cathode, a phenomenon that not only poses a serious threat the efficiency of the cell, but also leads to safety issues. In addition to this, the diaphragm must present a very low conduction to electrons to avoid the electrical shorts between the electrodes guaranteeing a small distance between cathode and anode.

The most common materials for this component are *composite materials* based on ceramic or microporous materials such as *polyethersulphone, glass-reinforced polyphenylene sulphide compounds* or *asbestos* (Rashid M.M., 2015). The latter is no longer used in recent applications for safety reasons.

All the components that characterize the conventional cell are separated from each other by some gaps that cause the increase of the ohmic losses. In recent years, electrodes with a zero-gap design directly pressed onto the separator have been developed to overcome this problem and to reduce both the drop in efficiency and the cell voltage. The most used materials are *Zirfon^{TM} Perl UTP 500* or dense anion exchange membranes and are characterized by a high porosity (Brauns J., 2020).

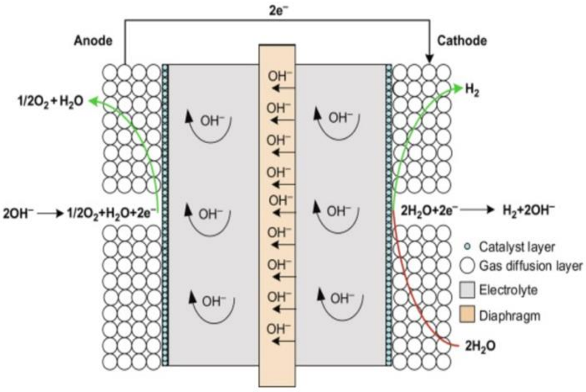

Figure 7: Water electrolysis in an Alkaline cell
(Chapter 9 - Electrochemical hydrogen generation, 2019)

As far as the electrodes are concerned, the decomposition of water into hydrogen and OH^- takes place inside the cathode. The hydroxide ions pass through the electrolyte and the diaphragm before reaching the anode where are oxidized to O_2 and water.

$$Anode\ reaction: 2OH^- \rightarrow\ 2e^- + \frac{1}{2}O_2 + H_2O \ (7)$$

$$Cathode\ reaction: 2H_2O + 2e^- \rightarrow H_2 + 2OH^- \ (8)$$

As it is possible to see in the figure below, besides the cell, the system is characterized by other components such as *pumps*, *heat exchangers, gas separators, drying* and *purification units*. Inside the cell, the electrolyte is pumped, and a consequent production of hydrogen and oxygen takes place. The generated two-phase mixture is sent to the *gas separator* where the liquid phase is separated to the gaseous one. After a long residence time inside these large containers, the produced gases are dried and finally purified to the desired level, while the liquid electrolyte is pumped back into the electrolysis cell.

In this type of system, it is advisable to use partially separated systems of the electrolyte cycles to prevent the produced gases from solubilizing within the electrolyte. The solubilization reaction can cause both higher losses and more impurities in the gases. The system just described requires equalization lines to balance the liquid level in the two tanks and maintain the optimum liquid conductivity level (Brauns J., 2020).

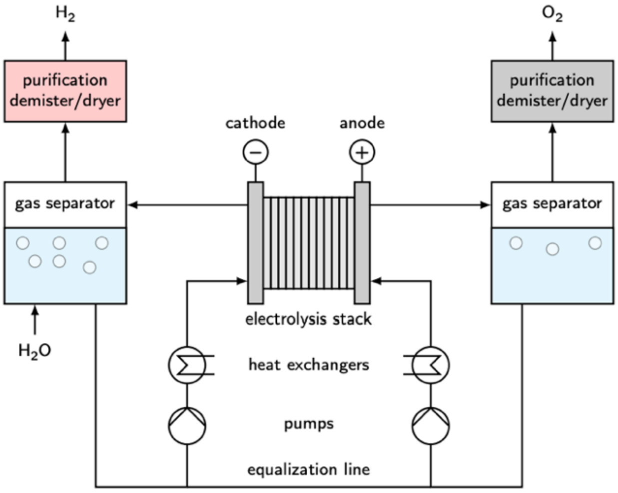

Figure 8: Complete alkaline electrolyzer system (Brauns J., 2020)

The produced gases must respect some strict purity requirements because in the range of 4 to 96% vol. of foreign gas contamination can cause the formation of explosive mixtures. The maximum technical safety limit before the emergency shutdown of the whole electrolyzer is a concentration of 2% vol. Generally, the hydrogen leaving the electrolyzer has a high purity (99.9% vol.) even without further purification, while the produced oxygen is characterized by purity values in the range of 99 to 99.5% vol. (Brauns J., 2020).

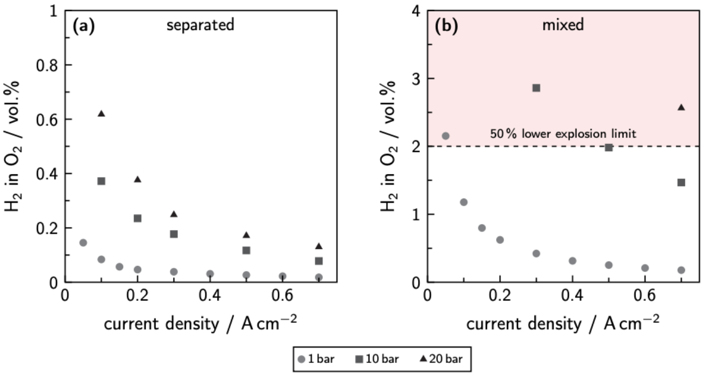

Figure 9: Anodic gas impurity evolution with respect to current density (Brauns J., 2020)

In the graphs above, it can be seen the clear difference in the volume percentage of hydrogen in oxygen between separate and mixed electrolyte cycles. In the former case, the volume percentage always remains below 0.7% for any current density and pressure, while in the second the percentage of impurities in the gas increases considerably.

In both graphs, impurities decrease with increasing current density and rise with increasing pressure. It can be also observed that at high current densities, contamination is more diluted and therefore the most dangerous operations are those at partial load.

From an economical point of view, the increase in pressure is a positive factor because it allows to avoid the compression of the hydrogen produced at the outlet of the electrolyzer and thus to save money. However, the pressure rise causes the increase of the concentration gradients for diffusion through the separator material and a consequent greater cross-over of the foreign gas to the other half-cell takes place (Brauns J., 2020).

2.2. Proton Exchange Membrane Electrolyzers (PEM)

The *polymer electrolyte* or *proton exchange membrane electrolyzers* similarly to the *AWEs* works at low temperature. More specifically, the operating temperature range is slightly wider than the previous case and varies from 50 to 80 °C (Shiva Kumar S., 2022).

However, the *PEMs* differ from the *AWEs* because the two electrodes are separated by perfluorosulfonic acid membranes and no more by a liquid electrolyte (Miller H.A., 2020). This membrane acts as a solid electrolyte and serves to separate the gases contained in the cathode and in the anode (Wang Y. Y. H., 2021). Unlike the Alkaline electrolyzers, only deionized water and no other additives are added to the electrolyte.

The components of the *PEM* are the *Membrane Electrode Assembly (MEA)* consisting of a membrane and the two electrodes with the electrocatalyst, the bipolar plates, the gas diffuser, and the gasket. The last two components are used to allow an electric current to flow to the *electrodes* and *bipolar plates.* The *bipolar plates* are made of titanium or coated stainless steel and are used to transport water at the anode and the product gases out of the electrolysis cell (Rashid M.M., 2015).

The membrane is the core component of the *PEM* cell and is usually made of perfluorosulphonic acid polymers such as *Nafion, Flemion* or *Fumapem.* Nowadays, the most used membranes are made of *Nafion 110, 115 and 117* and vary in thickness between 100 and 200 micrometres (Rashid M.M., 2015). In this range, the membrane exhibits high mechanical stability and gas permeability as well as small ohmic losses. These types of membranes have good durability, efficiency, and very good dimensional stability with temperature variation as well as oxidation stability.

Clearly, all these advantages such as the excellent thermal, mechanical, and chemical stability can only be achieved at high cost. Therefore, the membrane is very expensive and the only way to reduce costs and optimize production costs is by replacing the expensive material with a cheaper one or by reducing the load of the catalyst on the electrodes. For this reason, alternative membranes are being investigated to replace the current ones such as *bi-Phenyl Sulfone Membranes*, *Hydrocarbon Membrane* inexpensive starting materials and *PFSA* (Rashid M.M., 2015).

Usually, the membrane is directly coated with noble metal electrodes, whose oxides (IrO_2 in the case of iridium, RhO_2 in the case of rhodium) are used as electrocatalysts. Although the direct coating is the most widely used method, it is also possible to spray the electrocatalyst on the current collector and fix it subsequently with the electrode to the membrane.

The oxygen evolution reaction can be improved by using catalysts such as mixed oxides of ruthenium (RuO_2) and iridium (IrO_2) (Chi J, 2018). The former is the most active but still highly unstable, while the latter represent the right compromise between activity and stability. Much research has shown that RuO_2 and Ru undergo oxidation that results in RuO_4. After the oxidation reaction the Ruthenium precipitates, escapes from the catalytic membrane layer and its ions diffuse from the cathode to the gas passages. Despite of this limitation, Ruthenium oxides are much more abundant than iridium oxides and therefore researchers are trying to control their corrosive nature. The latest research results explain that one way to reduce the erosion rate by 4% and improve the stability of Ruthenium oxides is to mix the latter with IrO_2 (20%) (Rashid M.M., 2015).

PEM electrolyzers offer a lot of advantages with respect to *AWEs*. Firstly, *PEM* electrolyzers can produce a higher purity hydrogen gas and guarantee lower gas crossover through the diaphragm. In addition to this, they are characterized by a lower energy consumption, higher safety levels and easier handling and maintenance. Other non-negligible advantages are higher proton conductivity, smaller size, and reduced mass (Rashid M.M., 2015). These devices are also able to work at different pressures in the two electrodes, offering the possibility of using a high-pressure hydrogen flow in the cathode while maintaining an atmospheric pressure in the anode.

In addition, this technology features a faster response under an intermittent power supply and a more compact design due to the absence of a liquid electrolyte (Miller H.A., 2020). The biggest disadvantage of *PEMs* compared to *AWEs* is at the economic level and it is due to the need to use expensive catalysts such as noble metals (Ir, Ru or Pt) to guarantee high electrochemical stability in the corrosive acid medium where they must operate.

Another disadvantage concerns the hydrogen production at sea, as these electrolyzers are extremely vulnerable to the presence of ions such as Mg^{2+} and Ca^{2+}. Their precipitation in fact causes blistering, that is an irreversible damage to the MEA, which results in an efficiency decrease (D'Amore-Domenech R., 2020).

In the Figure 10, it can be seen the layout of the *PEM electrolyzer*. There, it can be distinguished several components, such as anode, cathode, diffusion layer and distribution plate.

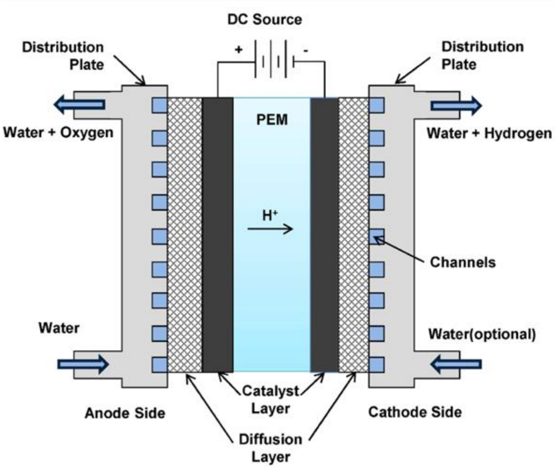

Figure 10: Water electrolysis in a PEM cell (Sood S., 2020)

Below, it can be highlighted the partial reactions that take place in both electrodes.

$$Anode\ reaction: H_2O \rightarrow \frac{1}{2} O_2 + 2H^+ + 2e^- \ (9)$$

$$Cathode\ reaction: 2H^+ + 2e^- \rightarrow H_2 \ (10)$$

The reaction of a *PEM* consists of splitting water into oxygen and hydrogen in the two electrodes. The water is pumped into the anode, where dissociation into oxygen, protons and electrons takes place.

The protons pass through the electrolyte on their way from the anode to the cathode, while the electrons pass through the external circuit. Inside the cathode, the recombination of protons and electrons takes place, resulting in the formation of hydrogen.

2.3. Anion Exchange Membrane Electrolyzers (AEM)

The anion exchange membrane electrolyzers represent a promising alternative to the low-temperature devices described above, because they aim to overcome the limitations of *PEMs* and *AWEs* by attempting to combine the advantages of both (Miller H.A., 2020).

In these cells, alkaline solutions with a low concentration of KOH or 1% K_2CO_3 are used to reduce the corrosiveness of the environment in comparison with *AWE* cells. The low KOH concentrations allow the use of less expensive materials such as Nickel and Cobalt for the electrodes as in *AWEs* and cheaper polymeric membranes than those used in *PEMs*. In addition to saving money, these membranes allow us to replace the diaphragm of the *AWE* and thus reduce gas cross-over between the electrodes. Two other important advantages of *AEMs* are the reduction of K_2CO_3 formation compared to *AWEs* and a low temperature operation range between 25-70°C (López-Fernández E., 2021).

Despite all these advantages, more in-depth studies on catalyst preparation methods and the search for optimal working conditions have yet to be developed. Optimization of these factors would lead to a further increase in the yield of these innovative cells.

An *AEM cell* consists of two corrosion-resistant bipolar plates with high electrical conductivity, two gaskets and a *MEA*. The most used material for the construction of bipolar plates is Nickel, but materials such as Titanium and Graphite can also be used in an alkaline environment. The gaskets are made of Teflon and have the dual function of electrical insulation and sealing between the two bipolar plates. The *MEA* consists of the two electrodes and the key element of the cell, which is the anion exchange membrane. The latter component must be characterized by thermal and mechanical stability and gas tightness to prevent the passage of gases or other by-products of the reaction inside the membrane. In addition, the MEA must also have excellent ionic conductivity to perform its main function of transporting hydroxide ions. This property can be enhanced through the nucleophilic substitution of ammonium groups or by the substitution of methyl groups by hydroxyl ions. The most used commercial membranes in *AEM* are *Fumasep® FAA-3*, *Sustainion® 37-50*, *Tokuyama A201*, *Aemion^{TM}* and *Orion^{TM1}* (López-Fernández E., 2021). As these membranes are supplied in bromide and chloride form, a pre-treatment by immersion in NaOH or KOH solutions prior to assembly in the cells is necessary. This process makes it possible to replace the Br^- and Cl^- ion with the hydroxide ion OH^- respectively.

The electrodes are made of an active catalyst phase deposited or distributed on a macroporous support or gas diffusion layer (*GDL*). The GDL has multiple functions, the most important of which are support for the catalytic phase and electronic conductivity between the catalyst sites and bipolar plates. In addition, this layer must be able to provide a removal pathway for the gaseous products of the two half-reactions and polarize the catalyst loads for these reactions to take place. For the anode, the *GDL* media can consist of Carbon paper or cloths, Ti papers, Stainless Steel felt or Ni foam. Nickel and Titanium as well as Stainless Steel are highly thermodynamically stable, while Carbon presents degradation problems because OH^- ions are excellent nucleophilic intermediates (López-Fernández E., 2021). On the other hand, concerning the cathode the most used materials for GDL supports are carbon paper, Ni, or stainless steel. In terms of catalyst materials, transition metals such as Co, Ni or Fe are used.

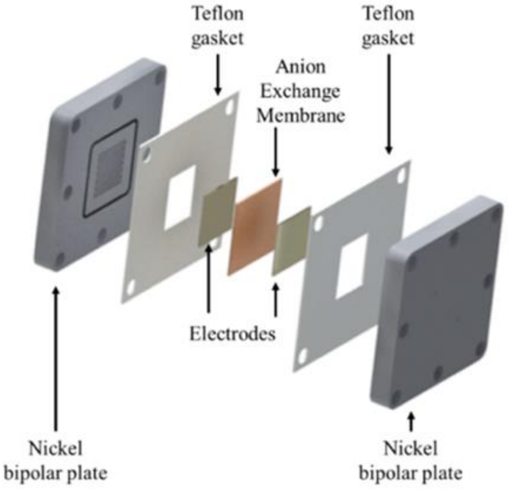

Figure 11: AEM cell assembly (López-Fernández E., 2021)

The chemical reactions in this cell are the same as those described above for *AWE cells* because both the electrolyzers use an alkaline electrolyte, albeit in different concentrations.

2.4. Solid Oxide Electrolyzers (SOE)

High energy consumption and low gas evolution rate are the major limitations in low temperature electrolyzers. To solve these problems and thus achieve better performance, high-temperature electrolysis reactions have been investigated in recent years (Brisse A., 2008).

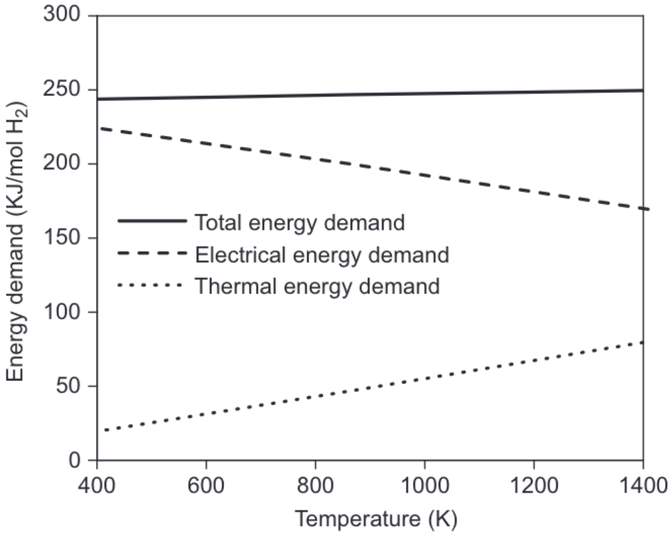

Figure 12: Evolution of the total energy demand as a function of temperature (Ni M., 2008)

In the graph above, it is possible to observe how an increase in the reaction temperature is followed by both an increase in thermal energy demand and a decrease in electrical energy demand. The two opposing trends result in the total energy demand remaining approximately constant as the temperature changes.

The advantage of high-temperature electrolysis is that the increase in thermal energy demand can be met through the coupling of high-temperature thermal plants with high waste heat such as nuclear reactors and renewable sources (Rashid M.M., 2015). However, high temperatures make the production of green hydrogen at sea complicated, as the only renewable source capable of providing high temperature heat is geothermal.

High temperature heat can be also recovered in Combined Heat Power (CHP) plants used for residential or industrial purposes, where a cogeneration process that produces electricity and heat at high efficiencies takes place. The utilization of waste heat in electrolyzers leads to an increase in process efficiency to values greater than 90% and a substantial reduction in energy consumption (Chi J, 2018).

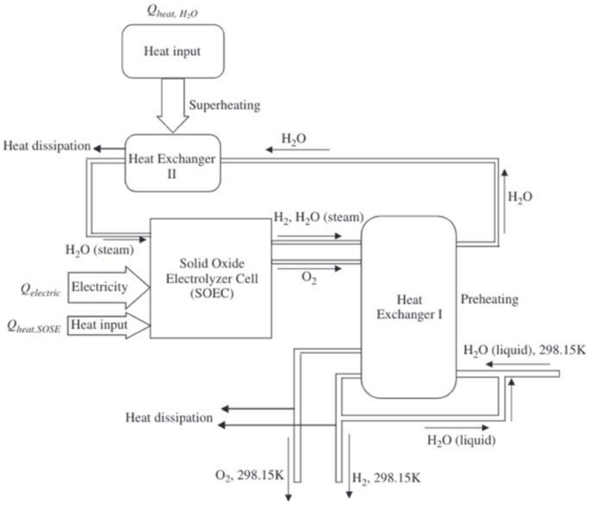

Figure 13: SOEC plant with waste heat recovery (Ni M., 2008)

To sum up, the reaction temperature increase has a twofold advantage: it improves the reaction kinetics increasing the reaction speed and reduces the energy consumption as less voltage is needed to reach the desired current density value (Shiva Kumar S., 2022). Although in many respects higher temperatures provide better performance, problems related to mechanical compatibility, thermal expansion and chemical stability of the various cell components must be considered. High-temperature reactions cause a higher degradation of materials which reduces the service life of the various components and can be only avoided by using stronger and consequently more expensive materials.

The most used high temperature electrolyzers are the *Solid Oxide Electrolyzers (SOE),* which are *Solid Oxide Fuel Cells (SOFC)* working in regenerative mode, or reverse mode. These electrolyzers work with water in the form of steam because they are characterized by an operating temperature range between 700 and 850°C (Shiva Kumar S., 2022).

In the *SOE*, the steam is supplied to the cathode, where it is reduced to pure hydrogen and oxygen ions. The H_2 molecules are separated at the cathode surface, while O^{2-} ions pass through the dense electrolyte to the anode, where they oxidize to form oxygen due to the recombination with electrons from the cathode (Nechache A., 2021).

$$Cathode\ reaction: H_2O + 2e^- \rightarrow H_2 + O^{2-} \text{ (11)}$$

$$Anode\ reaction: O^{2-} \rightarrow \frac{1}{2}O_2 + 2e^- \text{ (12)}$$

As can be seen in Figure 13, there is not only hydrogen among the cathode outputs. The accumulation of water in the cathode is one of the most common problems with *SOEs* and is due to osmotic diffusion, loss of membrane selectivity, oxidation reactions or excess moisture in the working environment. However, this inconvenient and the consequent membrane degradation and fouling can be solved using selective membranes, hydrogen compression or product cooling.

As in the *SOFCs* where different molecules can be oxidized because of the great fuel flexibility due to the high working temperatures, in the *SOEs* can be produced different fuels (CO, H_2, etc.). Besides water electrolysis reaction, these electrolyzers can be used both for the electrolysis of CO_2 and the co-electrolysis. Both reactions produce carbon monoxide, a fuel that can be used in various processes such as the methanol synthesis and the water gas shift to produce respectively methanol and hydrogen (Wang Y. L. W., 2020).

The difference between the two reactions is that co-electrolysis uses both water and carbon dioxide as inputs and so it is characterized by a co-production of hydrogen and carbon monoxide. This output fuel mixture is called syngas and can be used to generate electricity via Organic Rankine Cycle or steam turbine, to produce heat or steam for industrial purposes or to replace the conventional fuel in the boilers (VOW, 2023).

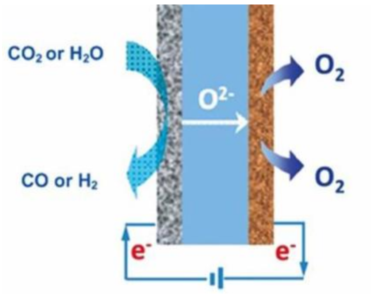

Figure 14: Water and Carbon Dioxide Electrolysis in a SOE cell (Wang Y. L. W., 2020)

In the case of electrolysis of CO_2, the reactions at the electrodes are:

$$Anode\ reaction\colon\ O^{2-} \rightarrow \frac{1}{2}O_2 + 2e^- \ (13)$$

$$Cathode\ reaction\colon\ CO_2 + 2e^- \rightarrow CO + 2O^{2-} \ (14)$$

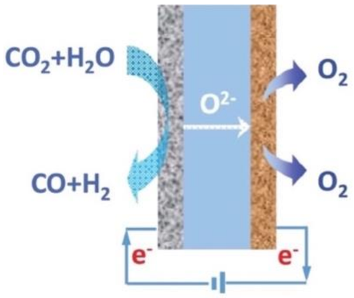

Figure 15: Co-electrolysis in a SOE cell (Zhang X., 2017)

In contrast, in the case of co-electrolysis:

$$Anode\ reaction: CO_2 + H_2O + 4e^- \rightarrow H_2 + CO + 2O^{2-} \quad (15)$$

$$Cathode\ reaction: 2O^{2-} \rightarrow O_2 + 4e^- \quad (16)$$

In terms of *SOE* materials, the electrolyte is a solid oxide or ceramic with high ionic conductivity. The most used material is ZrO_2 doped with 8% mol Y_2O_3, also called *yttria stabilized zirconia (YSZ)* (Nechache A., 2021). Zirconia is a material with high strength, skyscraping corrosion resistance and high melting temperature, while yttria is used to ensure greater stability. The addition of this material prevents the propagation of cracks and the decreasing conductive properties of the electrolyte (Bocanegra-Bernal M.H., 2002).

Regarding electrodes, the most used material for the anode *is lanthanum strontium manganate (LSM)* while that for the cathode is *nickel* doped with *yttria stabilized zirconia (YSZ)* (Nechache A., 2021). The alloy used for the anode can be impregnated with Gd-doped CeO_2 particles to increase the life of the cell by preventing problems such as delamination at the interface with the electrolyte (Chen K., 2010). Furthermore, this material offers high performance during the electrolysis process as it promotes oxygen diffusion through the generation of oxygen vacancies.

Perovskite-type LSM can also be used as a cathode material and can be doped with scandium to achieve higher performance and lower temperatures. The doping process is very useful as it increases the mobility of oxide ions in the fuel electrode, but scandium oxide precipitation in the *LSM* alloy lattice must be avoided because it can cause a decrease in both ion and electron conduction (Yue X., 2008).

2.5. Comparison between technologies

This section aims to compare the previously described electrolyzers to highlight advantages and disadvantages of each. The first major difference between these devices is the operating temperature range, which implies substantial changes in process reversibility, device lifetime, fuel flexibility and energy consumption. *PEMs* and *AWEs* work at temperatures of 60-80 °C, and 50-80°C respectively, while *SOEs* are characterized by higher temperatures and an operating temperature range between 700 and 850°C (Shiva Kumar S., 2022).

Process reversibility is strictly dependent on temperature and on the kinetics of the forward and backward reaction. The high-temperature devices such as *SOEs* can work both in fuel cell and electrolyzer mode, while for the low-temperature devices is still not possible to reverse the process.

As the temperature increases, the service life of the electrolyzer decreases because of material damage due to mechanical compatibility, thermal expansion, and chemical stability concerns. For this reason, *SOEs* are characterized by less than 20,000h of useful life, while higher values are reached for *AWEs* (60,000 - 100,000h) and *PEM*s (50,000 - 80,000h). On the other hand, the new *AEMs* are characterized by an operating lifetime higher than 30,000 hours (Shiva Kumar S., 2022).

Another difference between the electrolyzers concerns the fuel flexibility, which is higher increasing the temperature. Therefore, devices such as *SOEs* can perform both electrolysis and co-electrolysis processes, while low-temperature technologies such as *PEMs* and *AWEs* cannot because of carbon deposits issues.

The energy consumption is higher in *AWEs* and *PEMs* because they are characterized by higher voltages for the same current density due to the low temperature reaction. Increasing temperature implies a decrease in voltage and a consequent decrease in power consumption, resulting in greater energy savings and higher efficiencies. As it is possible to see in Figure 16, the specific energy consumption of the different electrolyzers is 4.1 - 4.76 kWh/Nm^3 H_2, 4.1-5.7 kWh/Nm^3 H_2, 3.70 kWh/Nm^3 H_2, 4.8 kWh/Nm^3 for *AWEs*, *PEMs* and *SOEs* and *AEMs* respectively.

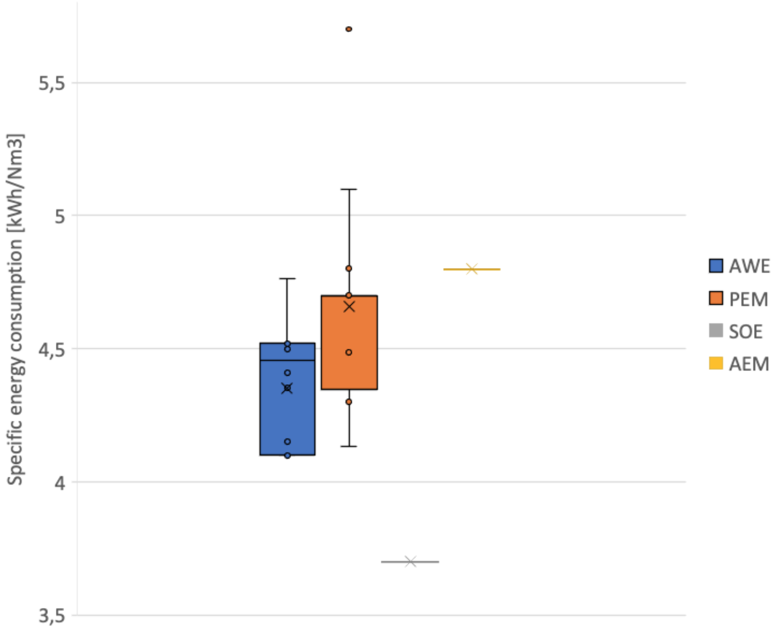

Figure 16: Commercial electrolyzers specific energy consumption

The box plot above have been elaborated with the data contained in the Table 32. The whiskers represent the maximum and minimum values, the box includes values between Q1 and Q3, the cross is the average value, the circles represent all the discrete values of the dataset, and the horizontal line in the box stands for Q2, that is the median.

On the other hand, the efficiency has an inverse trend with respect to the power consumption and can reach values of 89% for *SOEs*, while it is in the range 50-78%, 50-83% and 57-59% for *AWEs*, *PEMs,* and *AEMs,* respectively (Shiva Kumar S., 2022).

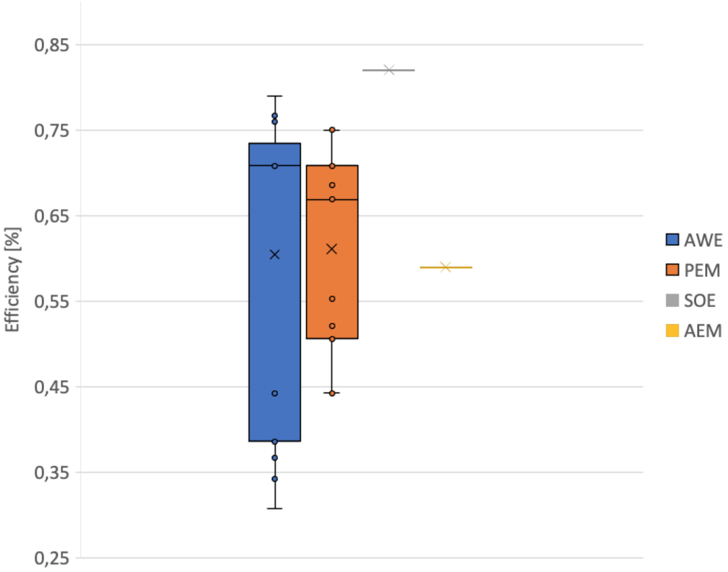

Figure 17: Commercial electrolyzers efficiency

The box plot above have been elaborated with the data contained in the Table 32. The whiskers represent the maximum and minimum values, the box includes values between Q1 and Q3, the cross is the average value, the circles represent all the discrete values of the dataset, and the horizontal line in the box stands for Q2, that is the median.

From Figure 6, it can be stated that as current density increases, investment costs decrease. Currently, the capital cost is about 500 \$/kWh for a mature technology such as *AWE* (D'Amore-Domenech R., 2020), 400 \$/kWh for *PEM*s, and is higher than 2,000 \$/kWh for *SOEs* (Shiva Kumar S., 2022). For the *AEMs* the capital costs of the stack are still unknown because it is a R&D stage.

Despite this, *PEMs, SOEs* and *AEMs* and can be used at much higher current densities than *AWEs*, and consequently the capital cost may decrease considerably in the future. More specifically, both *PEMs* and *AEMs* can reach current density levels of 2 A/cm^2, *SOEs* are characterized by values between 0.3 and 1 A/cm^2 while *AWEs* are limited to values between 0.2 and 0.8 A/cm^2 (Shiva Kumar S., 2022).

The cost of *SOEs* is currently higher due to lack of experience and knowledge than *AWEs* and *PEMs*, which have been commercially available for longer and nowadays represent the most mature technologies. As can be seen in Figure 18, both *AWEs* and *PEMs* are characterized by a *technology readiness level (TRL)* of 9, while *SOEs* and *AEMs* are still in the demonstration (*TRL* 7) and prototype (*TRL* 6) phase respectively (IEA, 2023).

Figure 18: Technology readiness level of the electrolyzers (IEA, 2023)

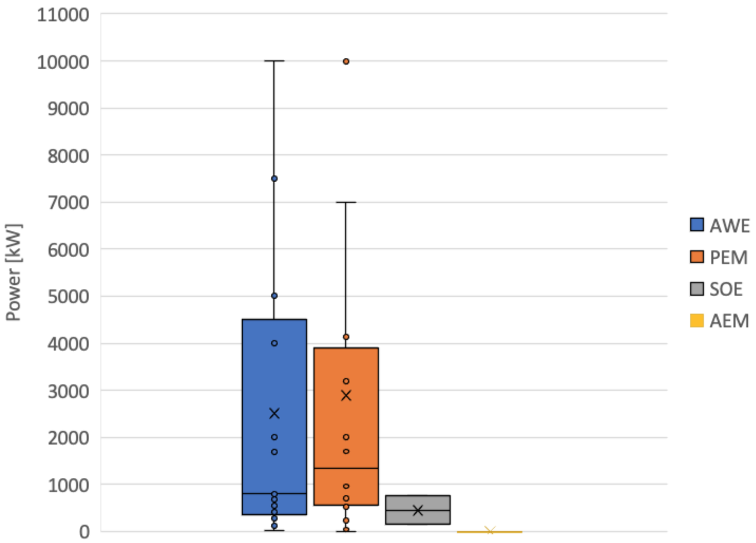

Figure 19: Commercial electrolyzers power

The box plot above have been elaborated with the data contained in the Table 32. The whiskers represent the maximum and minimum values, the box includes values between Q1 and Q3, the cross is the average value, the circles represent all the discrete values of the dataset, and the horizontal line in the box stands for Q2, that is the median.

At present, as Figure 19 shows, the market offers electrolyzers with powers in the order of MW in the case of *AWEs* and *PEMs*. On the other hand, commercially available *SOEs* can reach a few hundred kW, while *AEMs* being in the prototype stage have powers of a few kW.

The last difference worth mentioning is the variation in the cost of hydrogen as the device used changes. The cheapest devices are the *AWEs*, which achieve production costs of between 1.6 and 5 \$/kg H_2. This is followed by *PEMs* and *SOEs* with respective costs between 2.5 and 6.8 \$/kg H_2 and 2.8 and 5.8 \$/kg H_2 (Peterson D., 2016).

3. Hydrogen production from Seawater

3.1. Reference Seawater

Seawater is characterized by a variable composition over time and geographical location. Both atmospheric phenomena such as heavy precipitation, and proximity to glaciers or mixing with freshwater from rivers can alter salinity of sea or ocean water.

Nevertheless, seawater contains an average salinity of about 3.5%, which is approximately 35 grams of dissolved salts per liter of water (Millero F.J., 2007). In order to perform experiments in the laboratory with a consistent seawater composition, it is necessary to refer to a standardized composition of seawater.

Specifically, this work refers to the following *Reference Seawater*, characterized by the following solutes and composition:

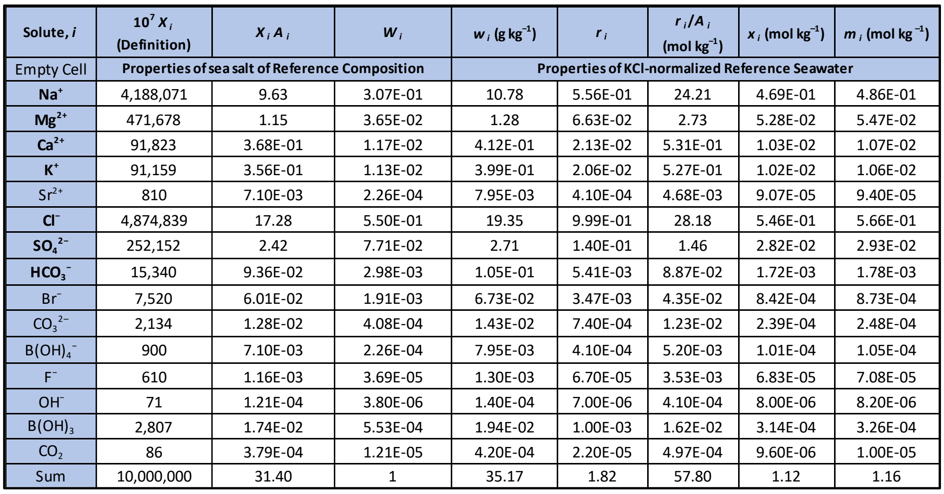

Solute, *i*	**$10^7 X_i$ (Definition)**	**$X_i A_i$**	**W_i**	**w_i (g kg^{-1})**	**r_i**	**r_i/A_i (mol kg^{-1})**	**x_i (mol kg^{-1})**	**m_i (mol kg^{-1})**
Empty Cell	**Properties of sea salt of Reference Composition**			**Properties of KCl-normalized Reference Seawater**				
Na^+	4,188,071	9.63	3.07E-01	10.78	5.56E-01	24.21	4.69E-01	4.86E-01
Mg^{2+}	471,678	1.15	3.65E-02	1.28	6.63E-02	2.73	5.28E-02	5.47E-02
Ca^{2+}	91,823	3.68E-01	1.17E-02	4.12E-01	2.13E-02	5.31E-01	1.03E-02	1.07E-02
K^+	91,159	3.56E-01	1.13E-02	3.99E-01	2.06E-02	5.27E-01	1.02E-02	1.06E-02
Sr^{2+}	810	7.10E-03	2.26E-04	7.95E-03	4.10E-04	4.68E-03	9.07E-05	9.40E-05
Cl^-	4,874,839	17.28	5.50E-01	19.35	9.99E-01	28.18	5.46E-01	5.66E-01
SO_4^{2-}	252,152	2.42	7.71E-02	2.71	1.40E-01	1.46	2.82E-02	2.93E-02
HCO_3^-	15,340	9.36E-02	2.98E-03	1.05E-01	5.41E-03	8.87E-02	1.72E-03	1.78E-03
Br^-	7,520	6.01E-02	1.91E-03	6.73E-02	3.47E-03	4.35E-02	8.42E-04	8.73E-04
CO_3^{2-}	2,134	1.28E-02	4.08E-04	1.43E-02	7.40E-04	1.23E-02	2.39E-04	2.48E-04
$B(OH)_4^-$	900	7.10E-03	2.26E-04	7.95E-03	4.10E-04	5.20E-03	1.01E-04	1.05E-04
F^-	610	1.16E-03	3.69E-05	1.30E-03	6.70E-05	3.53E-03	6.83E-05	7.08E-05
OH^-	71	1.21E-04	3.80E-06	1.40E-04	7.00E-06	4.10E-04	8.00E-06	8.20E-06
$B(OH)_3$	2,807	1.74E-02	5.53E-04	1.94E-02	1.00E-03	1.62E-02	3.14E-04	3.26E-04
CO_2	86	3.79E-04	1.21E-05	4.20E-04	2.20E-05	4.97E-04	9.60E-06	1.00E-05
Sum	10,000,000	31.40	1	35.17	1.82	57.80	1.12	1.16

Table 1: The relative contributions of all the major components for seawater (Millero F.J., 2007)

In Table 1, r_i represents the *ratio between the grams of solute and the kilograms of solution*, A_i is the *atomic weight*, X_i is the *mole fraction* from the observed stoichiometry of sea salt using the slightly adjusted values for Na^+ and CO_2. In addition, the ions marked in bold have been marked as the representative ions for synthetic seawater manufacturing in the lab.

Synthetic seawater was reproduced in laboratory by adding salts in different concentrations to a given amount of distilled water. More specifically, salts characterized by the ions Na^+, Mg^{2+}, Ca^{2+}, K^+, Cl^-, SO_4^{2-}, HCO_3^- were used because the other contributions are considered negligible.

From the solutes molar fraction, it is possible to derive the molar fraction of Na anions and calculate the molar fraction of salt molecules in seawater with the following equations:

$$x_{MgSO_4} = x_{SO_4^{2-}} \quad (17)$$

$$x_{NaHCO_3} = x_{HCO_3^-} = x_{Na^-} \quad (18)$$

$$x_{NaCl} = x_{Na^+} - x_{Na^-} \quad (19)$$

$$x_{MgCl_2} = x_{Mg^{2+}} - x_{SO_4^{2-}} \quad (20)$$

$$x_{CaCl_2} = x_{Ca^{2+}} \quad (21)$$

$$x_{KCl} = x_{K^+} \quad (22)$$

After that, the mole fraction of Cl cations is calculated through the sum of all the mole fractions of chlorine-containing molecules.

$$x_{Cl^+} = x_{NaCl} + 2x_{MgCl_2} + 2x_{CaCl_2} + x_{KCl} \quad (23)$$

By knowing the molar mass and the various molar fractions, it is then possible to estimate the different mass amounts of salt present in synthetic seawater.

$$m_i = x_i M_i \quad (24)$$

Some of these molecules ($MgCl_2$ $7H_2O$, $CaCl_2$ $6H_2O$, $MgSO_4$ $6H_2O$) are hydrated, so it was necessary to also calculate the mass amount of water in the molecule.

$$m_{water_{i*NH_2O}} = x_{i\,NH_2O} N\, MM_{H2O} \quad (25)$$

Where i represents a *generic salt molecule*, N represents the *stoichiometric coefficient of water* and MM_{H2O} is the *molar mass of water*. All molar masses of the salts are tabulated and have been taken from the web page of chemical manufacturers *ITW Reagents*, who produce high-quality chemicals for industrial processes (ITWReagents, s.d.).

Salt molecules	x [mol/l]	MM [g/mol]	m [g/l]	m_w [g/l]
NaCl	0.467	58.44	27.31	
$MgCl_2\ 6H_2O$	0.0246	203.3	5.00	2.66
$CaCl_2\ 6H_2O$	0.0103	219.09	2.25	1.11
KCl	0.0102	74.55	0.76	
$MgSO_4\ 7H_2O$	0.028	246.48	6.96	3.56
$NaHCO_3$	0.0017	84.01	0.14	

Table 2: Characteristics of salt molecules in synthetic marine water

To prove that the calculations were done in a correct way, a summation was made of all the mass quantities of the different salts.

$$m_{tot,salt} = \Sigma\, m_i - \Sigma\, m_{w,i} = 35{,}09\ g\ (26)$$

This result means that the laboratory synthetic seawater solution reproduces seawater very well as the salinity of the laboratory solution is very similar to the average salinity.

3.2. Hydrogen production at sea

The production of hydrogen at sea concerns the coupling of an offshore renewable source with an electrolyzer and can take place on marine platforms or on board a ship. Hydrogen can be carried onshore directly through the natural gas grid or through the electricity grid when an on-site fuel cell is used to transform previously stored hydrogen.

Saltwater electrolysis is an excellent solution to reduce the shortage of freshwater due to large-scale hydrogen production, because seawater is present on Earth in much larger quantities than freshwater, which is only found in glaciers, lakes, and rivers. More specifically, saltwater accounts for 96.5% of the water resources on Earth (Wang, 2022).

Electrolysis processes can take place with fully desalinated water or using saltwater directly. In the former case, the advantage is the use of an already state-of-the-art technology, but an increase in costs due to water treatment and desalination must be considered. Beside these drawbacks, it is also to be considered the disposal and the use of the removed residual salt. On the other hand, in the case of using seawater, the disadvantages are manifold as the technology is still being studied and all the chemical reactions increase proportionally to the presence of salt particles on the metal surface of the electrolyzer. There are three types of electrolysis that can occur in the presence of seawater, which differ according to the reaction products. The first one produces as outputs hydrogen and oxygen (Water electrolysis) and takes place at low current densities, while the second one (Chloralkali process) is characterized by the additional production of chlorine and alkalis (D'Amore-Domenech, 2021).

The *Chloralkali process* was born in the 19th century during the Industrial Revolution and quickly became the main process for producing chlorine (Cl_2), sodium hydroxide (NaOH) and hydrogen (H_2) through the sodium chloride (NaCl) electrolysis (Du F., 2018)

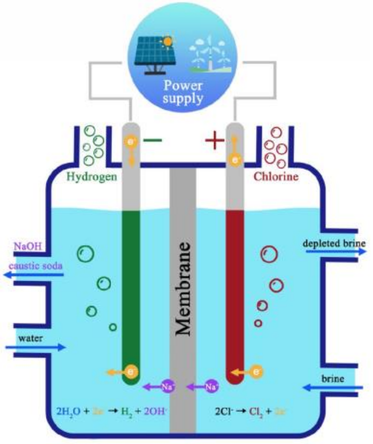

Figure 20: Chloralkali process configuration

(Fuel Cell Store, 2023)

$$Anode\ reaction:\ 2Cl^- \rightarrow\ Cl_2 +\ 2e^- \qquad E^0 = -1.36\ V \quad (27)$$

$$Cathode\ reaction:\ 2e^- + 2H_2O \rightarrow H_2 + 2OH^- \qquad E^0 = -0.83\ V \quad (28)$$

$$Overall\ reaction:\ 2NaCl + 2H_2O \rightarrow Cl_2 + H_2 + 2NaOH \qquad E^0 = -2.19\ V \quad (29)$$

Concerning the reactions, at the anode the chloride ions (Cl^-) lose electrons and are oxidized to chlorine (Cl_2) gas when saturated brine (NaCl) is added. On the other hand, the negative pole, that is the cathode, receives electrons and the reduction of water to hydrogen and hydroxide ions occurs. Between the two electrodes is the membrane, which allows sodium ions to pass through but prevents hydroxide and chloride ions. The Na^+ ions that cross the membrane react with the hydroxide ions at the cathode to produce sodium hydroxide (NaOH).

Nowadays, the old diaphragm cells composed of asbestos were substituted due to their environmentally hazardous toxicity with new diaphragm based on porous polytetrafluoroethylene (*PTFE)* or with membrane cells made of *Nafion*, *Flemion* or *Aciplex* characterized by higher efficiency. These membranes are called *ion-selective* because they allow the passage of Na^+ ions and block the negative ones. The main difference between these two cells is in the concentration of NaOH in the caustic bath, where membrane technology clearly outperforms diaphragm technology as can be seen in Table 3.

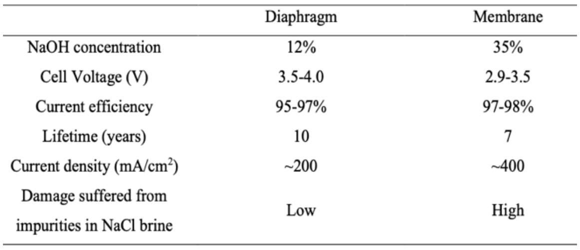

	Diaphragm	Membrane
NaOH concentration	12%	35%
Cell Voltage (V)	3.5-4.0	2.9-3.5
Current efficiency	95-97%	97-98%
Lifetime (years)	10	7
Current density (mA/cm^2)	~200	~400
Damage suffered from impurities in NaCl brine	Low	High

Table 3: Differences between diaphragm and membrane cells (D'Amore-Domenech, 2021)

Although this process is characterized by high energy consumption, the reaction products can be used for various purposes. Both chlorine and caustic soda are highly used in chemical industry as they represent commodity chemicals, while hydrogen is used to produce power or to produce other compounds such as ammonia, hydrogen peroxide and hydrochloric acid (Shreve R.N., 1977).

However, the most relevant application of this process is the production of NaOH at sea considering that the Alkaline electrolyzers represent the cheapest and the most efficient technology to produce green hydrogen offshore. The advantage is an easier replacement of the electrolyte in offshore applications that avoids the risks of manual substitution of caustic soda and the boat fuel consumption to reach the application site. In addition, hydrogen produced by the chloralkaline cell can be used to produce hydrochloric acid useful for removing precipitated deposits from the electrolysis unit and neutralizing soiled electrolyte for safer disposal (D'Amore-Domenech, 2021).

Unlike the two reactions previously described, the third reaction concerns the production of hydrogen and sodium hypochlorite (NaClO) and takes place when a direct current is applied to seawater. If Chloralkali and chlorate production reactions take place, the electrode material must be chosen carefully to avoid corrosion and subsequent dissolution of the anode in saltwater. Thus, the production of chlorate is not only dangerous for the environment, but also causes an increase in the cost of the anode, which must be made of a material with high chemical stability such as IrO coated Ti (D'Amore-Domenech, 2021). In addition, to prevent damages to the material's characteristics and physical properties it is important to monitor other parameters such as the presence of chloride, the temperature, and the production of chlorine.

In particular, the typical materials employed for the construction of electrodes due to their high nickel content such as stainless steel 316L cannot be used because they suffer serious damages during operation when in contact with hostile marine conditions. More specifically, when an anodic potential is applied, a high degree of corrosion occurs due to unwanted chlorine formations in the anode and undo the material.

Moreover, the presence of the anion SO_4^{2-} and of the cations Mg^{2+} and Ca^{2+} causes scaling, the formation of a solid layer on the materials of the electrolyzer, that can be minimized only by using ion exchange resins. In addition, periodic washes with acidic agents are mandatory to solve this problem. (D'Amore-Domenech, 2021)

Despite all these drawbacks, there are some advantages such as lower capital costs and an economic recovery of metals present in seawater which make this technology promising for future. The object of study for hydrogen production is the use of seawater with total dissolved salts in the 0.5-7% range (Abdel-Aal H.K., 2010). The typical *TDS* value of 3.5% in mass results in low ion conductivity which causes increased ohmic losses and a consequent increase in electrolyzer energy consumption. Therefore, direct seawater electrolysis cells are nowadays characterized by bigger dimensions and higher costs (D'Amore-Domenech, 2021).

3.3. Water purification

Water purification is carried out through the desalination process, which consists of removing the saline fraction from brackish or saltwater. This process enables us to obtain high quality water and thus meet the ever-increasing demand for freshwater for industrial, food or as cooling water.

A desalination plant consists of an intake system, a pre-treatment unit, a desalination plant, and a final post-treatment unit. The first component is used to take saltwater from the source and send it to the pre-treatment unit, where all solid components are removed, and chemicals are added to reduce salt precipitation and corrosion in the desalination unit. The final post-treatment unit receives the freshwater generated by the desalination unit to correct the pH by adding salts selected according to the end use of the water (Curto D., 2021).

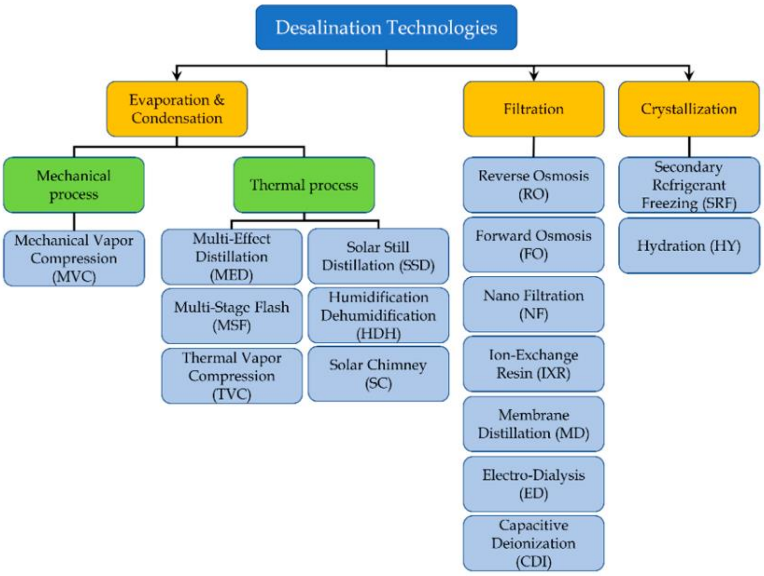

Figure 21: Desalination technologies (Curto D., 2021)

In the Figure 21, desalination technologies are subdivided into three categories: Evaporation and Condensation, Filtration, and Crystallization devices.

The first and oldest method involves the production of steam through the evaporation of water due to the application of an external heat source and subsequent condensation by means of a heat exchanger. The most used evaporation technologies are *Multi-Effect Distillation (MED)*, *Thermal Vapor Compression (TVC)* and *Multi-Stage Flash (MSF)*

(Saadat A.H.M., 2018). The steam production can be carried out by delivering thermal energy from waste heat or combustion of fuels, but it is possible to make the process more sustainable, by producing the thermal energy for evaporation through solar radiation, geothermal, and biomass energy.
In addition to the thermal processes just mentioned, freshwater can also be produced through mechanical ones, including *Mechanical Vapor Compression (MVC)*.

Nowadays, the most widely used technology concerns *Reverse Osmosis (RO)* Filtration devices, consisting of a semi-permeable membrane that can separate salts from water through the application of pressure. *Electrodialysis (ED)* and *Ion Exchange Resin (IXR)* can be used to produce freshwater but only if brackish water is involved, while the other filtration technologies are still in the development stage. To increase the sustainability of the process, these devices can be coupled with renewable sources that produce electricity, such as hydropower, wind, tidal, and wave (Curto D., 2021).

Finally, crystallization devices such as *Hydration (HY)* and *Secondary Refrigerant Freezing (SRF)* devices are still under study and development.

The contribution of each desalination technology in the market can be analyzed. As pointed out earlier, the most widely used process involves reverse osmosis, which accounts for 69%. This is followed by multi-stage flash distillation with 18% and multi-effect desalination with 7%. Electrodialysis accounts for only 2% of the total, while the remaining 4% sums up all the technologies still under development and study (Elsaid K., 2020).

The following table summarizes the characteristic parameters of the most important water distillation technologies, which are discussed in more detail in the next sub-chapter:

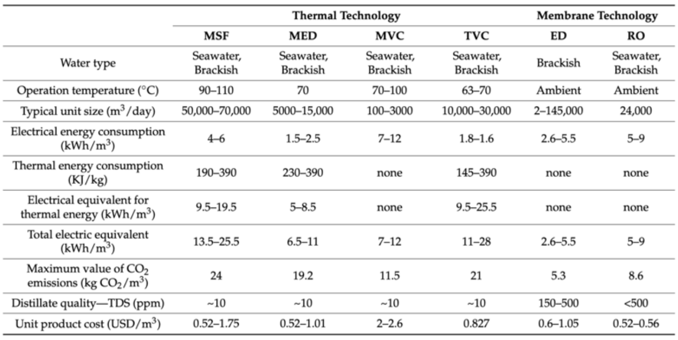

	Thermal Technology				Membrane Technology	
	MSF	**MED**	**MVC**	**TVC**	**ED**	**RO**
Water type	Seawater, Brackish	Seawater, Brackish	Seawater, Brackish	Seawater, Brackish	Brackish	Seawater, Brackish
Operation temperature (°C)	90–110	70	70–100	63–70	Ambient	Ambient
Typical unit size (m^3/day)	50,000–70,000	5000–15,000	100–3000	10,000–30,000	2–145,000	24,000
Electrical energy consumption (kWh/m^3)	4–6	1.5–2.5	7–12	1.8–1.6	2.6–5.5	5–9
Thermal energy consumption (KJ/kg)	190–390	230–390	none	145–390	none	none
Electrical equivalent for thermal energy (kWh/m^3)	9.5–19.5	5–8.5	none	9.5–25.5	none	none
Total electric equivalent (kWh/m^3)	13.5–25.5	6.5–11	7–12	11–28	2.6–5.5	5–9
Maximum value of CO_2 emissions (kg CO_2/m^3)	24	19.2	11.5	21	5.3	8.6
Distillate quality—TDS (ppm)	~10	~10	~10	~10	150–500	<500
Unit product cost (USD/m^3)	0.52–1.75	0.52–1.01	2–2.6	0.827	0.6–1.05	0.52–0.56

Table 4: Characteristic parameters of the main distillation technologies (Do Thi H.T., 2021)

3.3.1 Multi-effect distillation

This technology was first used in the 1950s but did not spread due to fouling problems on the pipes compared to other thermal-driven processes. A breakthrough was made in the 1980s, when applications at lower temperatures (<70°C) were designed to reduce this problem (Curto D., 2021). Nowadays this technology is used both to produce salt from saltwater and in the food industry to extract juice from sugarcane.

The energy efficiency of the multi-effect distillation device varies between 4 and 21% (Curto D., 2021) and is increased by supplying steam from waste energy sources of industrial processes or a steam turbine of a power plant. In addition to the steam supply component, the system consists of several chambers, heat exchangers, a condenser, a venting and a vacuum system.

The saline feedwater flow is divided into two parts, as depicted in Figure 22, to use the thermal energy of both freshwater and brine. In addition, this flow is used in the condenser as a refrigerant to allow condensation of the steam produced in the last chamber and the consequent production of freshwater.

The saline water heated in the condenser is led into the first chamber, where it rapidly evaporates due to the low pressure and the thermal energy supplied from outside. The produced steam moves upwards and is led by means of pipes to the next chamber, where it replaces the external heat source and allows the production of additional steam and brine from the saline feedwater. The brine remains at the bottom and can be discharged or transferred inside the other chambers characterized by decreasing pressures to force the extraction of more freshwater. The pressure should be lower and lower going forward with the chambers to ensure a lower boiling point. The process is the same in all the chambers and is repeated as many times as there are chambers until reaching the last chamber where all the steam is condensed to produce freshwater (Khawaji A.D., 2008).

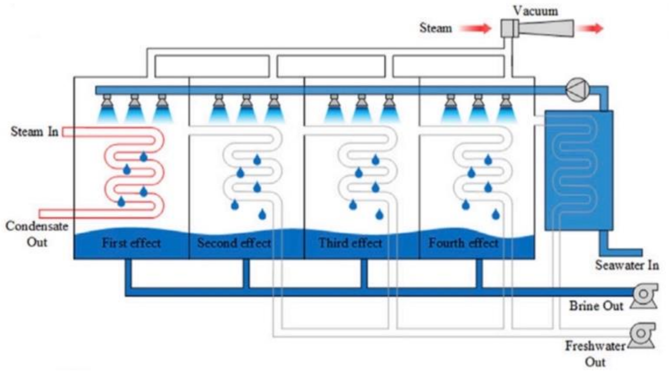

Figure 22: Multi-effect distillation system (Wang J., 2022)

The advantages of this technology are the very low energy consumption (< 1 kWh/m^3) compared to other thermal processes (Khawaji A.D., 2008), the high thermal efficiencies, the high reliability, and simplicity in the installation and operation. In addition, the maintenance and supervision costs are very low because it involves only few rotating parts. Furthermore, low temperatures make the coupling with power plants ideal and allow the use of any heat source including hot water technologies (Veolia, s.d.). Finally, the multi-effect distillation allows the production of high purity distillate without needing a pre-treatment of seawater.

The disadvantages of this technology are the high capital costs compared with the Reverse Osmosis process, as well as the large size of the *MED*. In addition, this technology requires a heat source to work, and it is not compatible with high temperatures because of scaling and fouling issues (Al-Obaidi M.A., 2022).

3.3.2. Multi-Stages Flash distillation

The Multi-Stage Flash was invented in 1950s in Scotland, but it spread very quickly because it provided easier maintenance operations than the *MED*. The *MSF* currently represents the most widely used desalination configuration among thermal processes, accounting for 18% of the total desalination capacity installed worldwide. Many countries such as USA and Korea use this technology to produce freshwater from seawater on ships and along the coastline (Curto D., 2021).

This technology allows water to be desalinated through multiple stages, which contain a countercurrent heat exchanger and a condensate collector. To maximize the efficiency of the system, these devices consist of 15-25 stages (Curto D., 2021). Before passing through the piping of the individual stages, the saline feed water is used as cooling water in the condenser. The saltwater heats up progressively until the maximum temperature is reached at the brine heater (90-120°C), where the saline feedwater is heated by a heat source such as steam spilled from a power plant (Khawaji A.D., 2008). The heat exchange with saltwater allows the steam to condense and its consequent reuse in the power plant. On the other hand, the hot saltwater is sent back into the lower part of the first stage where lamination occurs, and vapor is produced.

The steam is warmer than the saline feedwater and through a heat exchange it condenses producing freshwater that is led to the successive chambers. The brine remains in the lower part, and it is transferred to the other chambers, where it is again laminated due to the progressive pressure drop. The continuous pressure decrease is crucial to force steam production as it produces the so-called *flashing effect*, which allows a quick evaporation of the saline water in the chambers (Curto D., 2021).

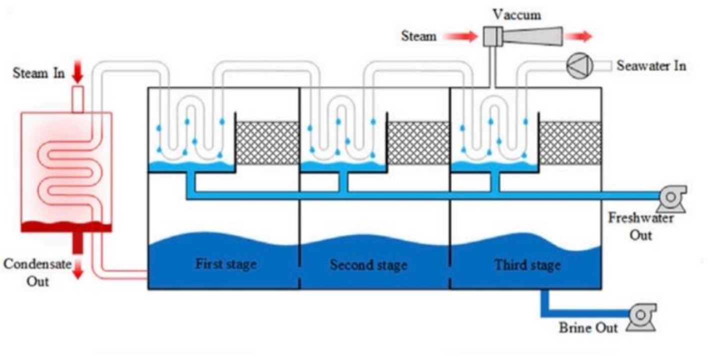

Figure 23: Multi-Stages Flash desalination system (Wang J., 2022)

The advantages of this technology are the low operating costs when using an external waste heat source and the ability to use even less high-quality feedwater than reverse osmosis. The saline feedwater in this case may then contain contaminating particles such as suspended solids, heavy metals, and oil.

On the other hand, the disadvantages of this process are the higher scaling and corrosion due to high temperature in comparison with the Multi-Effect Desalination, the higher capital cost, and the less compactness with respect to Reverse Osmosis devices. In addition, it is considered a very energy intensive process as its specific energy consumption is higher than the one of the other desalination technologies. Finally, as well as *MED*, a high-temperature heat source is required for the process to occur (Al-Obaidi M.A., 2022).

3.3.3. Reverse Osmosis

Reverse osmosis is a water purification process that allows the remotion of many types of chemical and biological species to obtain freshwater. To achieve the separation, this technology involves the use of a semi-permeable membrane that only allows certain molecules to pass through (Elga Veolia, 2021).

Normally, when two solutions with different concentrations are separated by the membrane and no external forces are applied the Forward Osmosis occurs. More specifically, the solvent moves spontaneously from the more diluted to the more concentrated part to balance the energy potential of the solutions (Mohammadifakhr M., 2020)

However, it is possible to reverse the motion by applying an external pressure greater than the osmotic pressure to the more concentrated side. This quantity is defined as the value capable of stopping the spontaneous motion of the solvent and can be calculated as follows:

$$p_{osm} = i[c]R\tau \quad (30)$$

Where i is the *van't Hoff index*, [c] is the *molar concentration of the solute*, R is the *ideal gas constant* and τ is the *absolute temperature of the solution.*

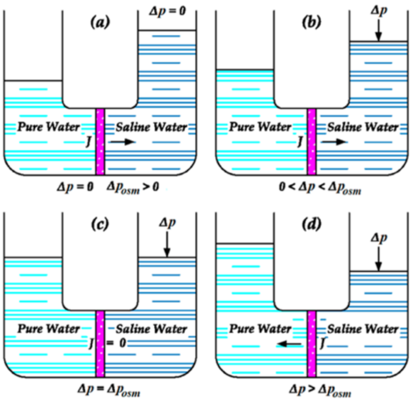

Figure 24: (a) Forward Osmosis, (b) Retarded osmosis, (c) Zero flow, (d) Reverse Osmosis (Curto D., 2021)

In the case of flow reversal through the application of external pressure, the process is called Reverse Osmosis and the solvent can be extracted from the more concentrated side to obtain pure water beyond the membrane.

This process can be used for saltwater desalination and requires electrical or mechanical energy to run the pumps, that raise the pressure of the saltwater. More specifically, for the flow reversal pressures between 15 and 25 bar are needed for brackish water and between 54 and 80 bar for saltwater. Through the application of the operating conditions, Recovery Ratio (RR) values of between 35 and 50% are obtained. This value could be increased by applying higher pressures before the semi-permeable membrane, but with current technology this is not possible due to problems with the mechanical resistance of the membrane (Curto D., 2021).

Among the advantages, this technology enables complete water purification as it can extract 99% of Total Dissolved Solids (TDS) from water. It is also a more compact and less expensive technology that requires less space and maintenance than other technologies on the market (Al-Obaidi M.A., 2022).

On the other hand, the disadvantages of this technology are the need to change and maintain filters, the high installation costs, and the possibility of system clogging or fouling (Vedantu, s.d.). Finally, this desalination process is not very efficient at high salinity levels and possesses lower productivity than thermal processes and it requires high pressure pumps and piping system to drive water (Al-Obaidi M.A., 2022).

3.3.4. Electrodialysis

Electrodialysis is an electrochemical desalination method invented in 1890 by Maigrot and Sabates and developed industrially about fifty years ago. This process is based on ion exchange semipermeable membranes due to their high-water recovery without the use of phase changes, reactions, or chemicals (Al-Amshawee S., 2020).

Dissolved ions are removed from the solution by generating through the electrodes an electric field that allows them to separate from the freshwater. The electric field generates an electric-type force on the particles, which is directly proportional to the amplitude of the field and the charge of the ion. More specifically, the positive ions are attracted to the negative pole, the anode, while the negative ones are attracted to the positive pole, the cathode. Many semipermeable membranes called cationic and anionic are installed between the two electrodes and can selectively block the migration flow of anions and cations, respectively. The ions are then collected within the salt channels, and the freshwater is extracted without impurities through another channel (Curto D., 2021).

This technology has the advantage of not using chemicals and fossil fuels, avoiding the pollution of the environment. Other advantages of electrodialysis are the ability to distinguish ionized from non-ionized components and the absence of phase changes, which result in lower energy consumption.

However, this technology presents some drawbacks regarding scaling, membrane fouling and permselectivity (Al-Amshawee S., 2020). Another disadvantage concerns clogging of the device, which can be reduced through feedwater pretreatment, and the system incapacity to remove organoid debris, colloids, and silicon dioxide (NetSol Water, 2022).

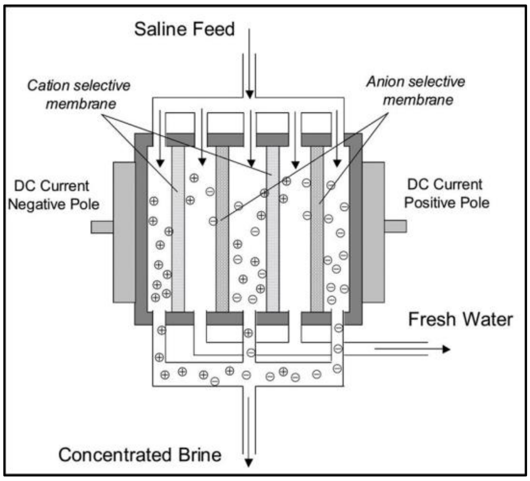

Figure 25: Electrodialysis desalination system (Saadat A.H.M., 2018)

Nowadays, electrodialysis is only used to remove ions in brackish water with a salinity up to 2,000 ppm, as the same process with seawater is considered energy intensive. However, energy consumption can be reduced by dividing the process into several stages so that each part of the system can work at its optimum operating point (Doornbusch G.J., 2019). Desalinated brackish water exiting an electrodialysis device has very high qualities, so only minimal pretreatment concerning a chlorination process for disinfection is necessary (NetSol Water, 2022)

4. Materials and Methods

This chapter explains all the component materials of the laboratory-designed alkaline electrolyser, such as the materials used to design the cell with the 3D printer, the materials of the prefabricated components and the electrolyte.

In addition, it defines the case study by showing all the technical assumptions and evaluations that were made to obtain an economic evaluation of a commercial alkaline electrolyser and shows a methodology to quantify the additional cost of handling the electrolyte.

This chapter also shows the methodologies used during the experimental phase of the thesis relating to the distillation, construction and assembly of the cell and the final production of hydrogen in the laboratory.

4.1. Materials of the cell

- **Polylactic acid (PLA) – $(C_3H_6O_3)_x$:**

This material is one of the most widely used materials for 3D printing because in addition to being inexpensive it provides good printing performance at low temperatures and does not require a heated bed. In the laboratory, this material was used for the support structure, which was removed by a bath in NaOH solution.

Polylactic acid is also considered an environmentally friendly plastic material as it comes from processing plant products such as potatoes and corn. In addition, although this material is not normally biodegradable it is possible to make it become so by subjecting it to hydrolysis at temperatures greater than 60°C and humidity greater than 20%.

The biodegradation time of polylactic acid is of about 1-4 years and it is significantly less than that of commonly used plastic materials, which take up to 1,000 years to degrade. PLA is also characterized by high stiffness, good strength, and a long service life. Despite all these advantages, this material is unusable in applications subjected to excessive heat sources because of its low melting temperature (Felfil, s.d.).

Figure 26: Polylactic acid for 3D printing (MatterHackers, s.d.)

- **Polypropylene (PP) – $(C_3H_6)_x$:**

It is a thermoplastic polymer that is obtained from the polymerization of propylene. This can be used for the construction of vehicle parts, industrial materials, and electronic components. The great advantages of this material are low density, high mechanical strength even under fatigue, and low moisture absorption, which allows it to be used in water applications.

Polypropylene can also work both at high temperature as it is characterized by a high melting point and with acidic substances such as alkaline due to its high chemical resistance. In addition, this material is also capable of acting as an electrical insulator (envaselia, s.d.).

Figure 27: Polypropylene filament for 3D printing (KREAfil, s.d.)

- **Polyvinyl alcohol (PVA) – $(C_2H_4O)_x$:**

It is an odorless, non-toxic, and biodegradable synthetic polymer characterized by excellent adhesive properties, as well as high tensile strength and flexibility. It is created by polymerizing vinyl to be used in industrial applications such as papermaking, textiles, and printing (Medicine, 2023). In the laboratory, it was intended to be used as a support structure, but due to its hygroscopic nature, the supports started to fail in thin pieces because of the high-water content in the PVA spool.

Beyond polymerization, PVA must be hydrolyzed to obtain filaments intended for use as print supports in 3D printers. Before use in the 3D printer, it is necessary to preheat the build plate to between 45-60 °C and to bring the extruder to a temperature range of 180-200 °C (natives, 2022).

Among the disadvantages of this material, it can be highlighted its high cost considering that it is a material that dissolves in post-processing and its high sensitivity to moisture. Therefore, to avoid generating undesirable changes in its properties, it is necessary to store it in highly controlled environments.

Figure 28: PVA before and after hydrolysis

- **Photopolymer Resin:**

This material was used in the laboratory for the creation of dimensionally accurate mock electrodes while waiting for the stainless-steel ones and for testing the watertightness with O-ring seals.

The photopolymer resin is stored in a reservoir on which it impinges an ultraviolet light pattern that corresponds to all parts of the print file. When the photopolymer has been cured, a solid layer is formed, and the bed is repositioned for the next layer to be printed (Hatchbox, s.d.).

The photopolymer resin is light sensitive and must be protected from direct sunlight and room light. Furthermore, this material must be stored in environment characterized by a temperature range between 15 and 25°C and consumed within 9-12 months. In addition, it must be handled carefully because can cause both skin and eye irritation and it is advisable not to breathe its dust, fume, or spray.

Figure 29: Laboratory Zortrax resin 3D printer

- **Gold and Brass:**

These are the materials that make up banana plugs. Specifically, gold is used for the outer part, while brass makes up the inner part of these components. These are two different materials in that gold (Au) is a transition metal, while brass is an alloy of copper (Cu) and zinc (Zn).

The former is characterized by its yellow color and a great chemical inertness that allows its use even in the presence of moisture, heat, acids, and caustic alkalis. In addition, being the metal that conducts electricity best and being little susceptible to oxidation phenomena, it is used for contacts or conductors of microscopic size.

On the other hand, brass has good corrosion resistance as well as high values of hardness, resilience, and fusibility. It is to be emphasized that both materials are characterized by high malleability and ductility.

Figure 30: Gold and brass banana plug

- **Stainless Steel:**

This material has been used for the construction of electrodes because it is characterized by high resistance to oxidation and corrosion. It can therefore also be used in the case of an alkaline electrolyzer using caustic soda as the electrolyte.

Stainless steel is an alloy of iron and is composed in part of an element such as chromium (12-18%) that can prevent the oxidation of iron. This phenomenon known as passivation is due to the formation of a thin coating due to the oxidation of chromium, which protects it from attack by chemicals and oxygen.

In the specific laboratory case, it was used 316L stainless steel because it is characterized by a high nickel content that helps to improve the oxygen evolution reaction and makes this material a suitable candidate for alkaline electrolysis. More specifically, stainless steel is characterized by these weight percentages of the constituent elements of the alloy: *Cr (16,5/18,5%), Ni (10,5/13,5%), Mo (2/2,25%), C (< 0.02%).*

- **Sodium hydroxide (NaOH):**

This material, also called caustic soda, remains solid at room temperature, and is characterized by strong hygroscopicity and deliquescence.

Sodium hydroxide is therefore able to quickly absorb the water molecules around it and dissolve to form a solution until equilibrium between the vapor pressure of the aqueous solution and the partial pressure of water in the atmosphere in contact with it is reached.

The NaOH solutions are used to neutralize acids in various commercial process. Although this salt is the most widely used industrial alkali, it should be handled with care as it is highly corrosive to animal and plant tissue (Britannica, 2022).

Figure 31: NaOH (Britannica, 2022)

4.2. Definition of the case study

The case study concerns the economic evaluation of an assumed commercial alkaline electrolyzer connected to the national power grid, which supplies the electricity required for continuous water electrolysis.

It is assumed that the plant is placed in the sea, 5 km off the western Sicilian coast of Mazzara del Vallo, as there is already a pipeline called the Trans-Mediterranean pipeline linking Algeria with Italy and Slovenia at this site. This currently allows the transport of natural gas between the African continent and the European continent, but in the future, it can be exploited for the transport of hydrogen.

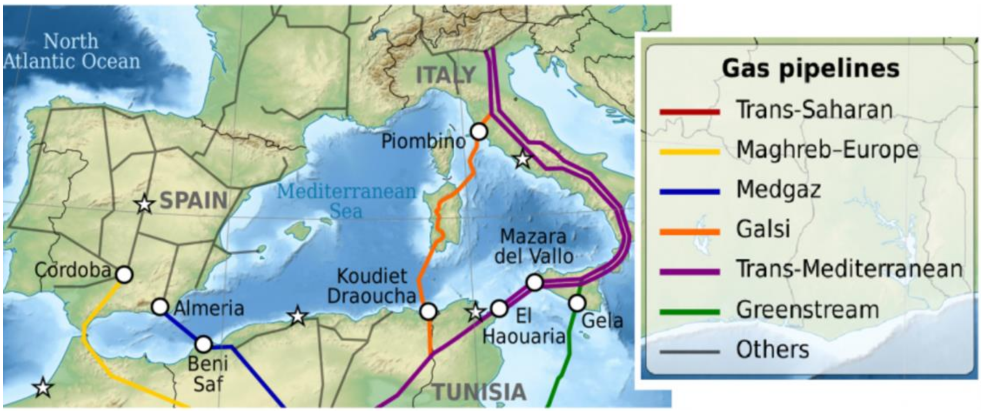

Table 5: Natural gas pipelines in Italy

It is therefore assumed that this existing pipeline can be used for the case study installation and that that the few additional costs for transporting hydrogen to the mainland are only related to the civil works involved in its adaptation. It is also assumed that one can have continuous access to seawater and that the costs of seawater are perfectly balanced by Italian state incentives and the sale of Emissions Trading Systems, as it is a green hydrogen production plant.

Before the plant is built, however, it is necessary to apply for permits and authorizations from the relevant authorities, such as the Harbor master's Office of the province, the Marine Protected Area Management Authority, and to check local regulations.

4.2.1. Technical assumptions

The first step in the technical assumptions' definition of the alkaline electrolyzer is the choice of hydrogen production in our plant.

$$\nu_{H2} = 440\frac{Nm^3}{h} = 38.72\frac{kg}{h} = 339{,}187\frac{kg}{y}$$

Considering this hydrogen production, it is immediately possible to calculate the hourly amount of water consumed according to a mass balance.

$$\nu_{H2O} = 9\,\nu_{H2} \quad (31)$$

In this analysis the current density is kept the same as in the laboratory case (j = 0.3 A/cm^2) and the stack size is chosen based on the current size of commercial electrolyzers. With these data, it is possible to calculate the area (A) and subsequently the current density flowing into the stack.

$$A_{stack} = \frac{\pi d_{stack}^2}{4} \quad (32)$$

Where d_{stack} is the length of the stack and it is equal to 150 cm, according to length of commercial alkaline electrolyzers.

$$I = jA_{stack} \quad (33)$$

Having obtained the current intensity, it is possible to calculate the number of the series cells (n_c) required to guarantee this hydrogen production.

$$n_c = \frac{\nu_{H2} z\, F}{\eta_F\, I} = 199 \quad (34)$$

Where z, F and η_F are the same as the laboratory case. This is an acceptable value as there are already commercial stacks with this number of cells in series (Ruth M., 2017).

The next step is to calculate the voltage of the stack (V_{stack}), which in the case of cells in series is equal to:

$$V_{stack} = V_c n_c \quad (35)$$

Where V_c is the voltage of the cell and for an alkaline electrolyzer varies between 1.8 and 2.4 V. In this case, a value of 2 V is chosen (Zhang F., 2016).

The current intensity of the stack is equal to that of the individual cell because the cells are connected in series. Knowing this value and the voltage of the stack, it is then possible to estimate the power consumed (W_{stack}) to carry out the water electrolysis reaction.

$$W_{stack} = V_{stack}\, I \qquad (36)$$

Finally, the efficiency in relation to the higher heating value (η_{HHV}) and the losses due to heating the cell (Q) are evaluated as follows:

$$\eta_{HHV} = \frac{v_{H2} HHV}{W_{stack}} \qquad (37)$$

$$Q = W_{stack}\left(1 - \eta_{HHV}\right) \quad (38)$$

After evaluating the energy variables, the volume and weight of the electrolyte and water inside the electrolyzer are calculated. To perform these calculations, a separation distance between the cells (δ_{sep}) is assumed to be equal to 1 cm.

The volume of the electrolyte (V_{NaOH}) is determined by adding the total volume of the separation spaces between the cells (V_{sep}) and the volume of the NaOH reservoir (V_{res}), that is estimated equal to 7.57 m^3 from values found on tank manufacturer websites (Protank, 2023).

$$V_{sep} = \delta_{sep}\, A_{stack}\, n_c \quad (39)$$

$$V_{NaOH} = V_{res} + V_{sep} \quad (40)$$

Having determined the volume of the electrolyte and knowing the density value of NaOH (2,180 kg/m^3), the weight can be determined as follows:

$$m_{NaOH} = V_{NaOH}\, \rho_{NaOH} \quad (41)$$

The electrolyte solution consists of 20% sodium hydroxide and 80% water. Therefore, knowing the weight of the electrolyte, it is possible to also derive the weight of the water (m_{H2O}) through a simple proportion.

$$m_{H2O} = m_{NaOH} \frac{0.8}{0.2} \quad (42)$$

Therefore:

$$V_{H2O} = \frac{m_{H_2O}}{\rho_{H2O}} \quad (43)$$

Where ρ_{H2O} is the density of water and is equal to 1,000 kg/m^3.

In the table below all the results obtained by the technical evaluation:

d_{lab} [cm]	2
A_{lab} [cm2]	3.14
d_{cs} [cm]	0.754
d_{stack} [cm]	150
A_{stack} [cm2]	17,671.5
j [A/cm2]	0.3
I [A]	5,301
n_c	199
V_c [V]	2
V_{stack} [V]	397.4
W_{stack} [MW]	2.11
η_{HHV}	0.739
Q [MW]	0.55
δ_{sep} [cm]	1
V_{NaOH} [m3]	11.08
V_{H2O} [m3]	96.62
m_{NaOH} [kg]	24,157
m_{H2O} [kg]	96,627
ν_{H2} [kg/h]	38.72
ν_{H2O} [kg/h]	348.48

Table 6: Key parameters of the electrolysis stack

4.2.2. Economic evaluation

The economic evaluation begins by researching the relative costs of the plant, which include the investment costs for the alkaline electrolyzer, the electrolyte, and the hydrogen storage.

More specifically, sodium hydroxide and electrolyzers relative costs are equal to 1 €/kg and 500 €/kW$_{el}$ respectively, while the hydrogen storage CAPEX range between 375 and 490 €/kg (Gorre J., 2020) (D'Amore-Domenech R., 2020).

For a correct assessment of the life cycle of the system, the relative cost of replacing the stack must also be evaluated. The value in the table below comes from technical specifications for water electrolysis (Nguyen T., 2019).

As this is an offshore green hydrogen production from seawater, it is also necessary to know the relative cost of distillation and the average cost of electricity from offshore renewable sources. The former varies in a range between 0.64-0.83 €/m^3 (Wade M., 2000), while the latter refers to an average data of 2021 provided by the Italian public body *Gestore dei Servizi Energetici* (*GSE)* and related to renewable sources such as solar and wind.

It is important to specify that in the analysis, the electricity price c_{el} of two years ago was chosen over today's as it currently has very high values due to the war in Ukraine. If the current price were taken into account, the price of the plant would increase dramatically and make the plant economically unfeasible.

Distillation costs [€/m3]	0.73
NaOH cost [€/kg]	1
Hydrogen storage CAPEX [€/kg]	382.5
AWE CAPEX [€/kWel]	500
Stack replacement costs [€/kWel]	340
Electricity cost [€/kWh]	0.07

Table 7: Relative costs of the plant

All the values in Table 7 represent average values for the previously mentioned ranges. From these, it is possible to calculate the absolute values of fixed capital costs and plant operating costs as follows:

$$C_{NaOH} = c_{NaOH}\, m_{NaOH} \qquad (44)$$

Where C_{NaOH} and c_{NaOH} are the absolute and relative cost of the electrolyte respectively, m_{NaOH} is the electrolyte mass.

$$C_{storage,CAPEX} = c_{storage,CAPEX}\, \vartheta_{H2} \qquad (45)$$

Where $C_{storage,CAPEX}$ and $c_{storage,CAPEX}$ are the absolute and relative hydrogen storage investment cost respectively, θ_{H2} represents the hydrogen storage capacity and is considered equal to 1000 kg so that it can contain the hydrogen produced in one day.

$$C_{AWE,CAPEX} = c_{AWE,CAPEX}\, W \qquad (46)$$

Where $C_{AWE,CAPEX}$ and $c_{AWE,CAPEX}$ are the absolute and relative investment cost of the alkaline electrolyzer respectively and W is the consumed power for water electrolysis.

$$C_{sr} = c_{sr}\,W \qquad (47)$$

Where C_{sr} and c_{sr} are the absolute and relative costs of the stack replacement.

The investment costs for the distillation plant and compressor are found on a vendor site (Alibaba.com, 2023) and in a University of Nebraska publication (Richardson I., 2015) , respectively.

By adding up these values, the total fixed costs (C_{fixed}) are obtained, which is useful for determining indirect costs:

$$C_{fixed} = \sum C_{i,fixed} \qquad (48)$$

$$C_{sp} = 5\%\,C_{fixed} \qquad (49)$$

$$C_{ed} = 10\%\,C_{fixed} \qquad (50)$$

$$C_{pc} = 5\%\,C_{fixed} \qquad (51)$$

$$C_{lf} = 0.1\%\,C_{fixed} \qquad (52)$$

$$C_{uf} = 3\%\,C_{fixed} \qquad (53)$$

Where C_{sp} are the site preparation costs, C_{ed} are the engineering design costs, C_{pj} are the project contingency costs, C_{lf} are the one-time licensing fee costs, and C_{uf} are the up-front permitting costs (Nguyen T., 2019).

After obtaining the contribution of each of the indirect costs, it is possible to find the total indirect costs ($C_{indirect}$) and the CAPEX of the plant (C_{CAPEX}).

$$C_{indirect} = \sum C_{i,indirect} \qquad (54)$$

$$C_{CAPEX} = C_{fixed} + C_{indirect} \qquad (55)$$

$$C_{CAPEX,y} = \frac{C_{CAPEX}}{N_y} \qquad (56)$$

Where $C_{CAPEX,y}$ is the yearly CAPEX cost and N_y represents the years of operation of the plant and is equal to 12 years.

The number of years of the system is chosen because an alkaline electrolyzer has a lifetime of about 100,000 hours. In this case, the system will run at full power for 105,120 hours.

After that, the operational and maintenance costs of all plant devices are determined as follows:

$$C_{dist,op} = \frac{c_{dist} \ \nu_{H2O} \ N_y}{\rho_{H2O}} \qquad (57)$$

Where $C_{dist,op}$ and c_{dist} are the absolute and relative operational costs of the distillation respectively and ν_{H2O} represents the yearly water consumption.

$$C_{el} = c_{el} \ W \ N_y \ N_{hours,y} \qquad (58)$$

Where C_{el} and c_{el} are the absolute and relative electricity costs respectively and $N_{hours,y}$ represents the number of hours per year.

$$C_{compr,op} = \eta_{compr} \ c_{el} \ N_y \ \nu_{H_2} \qquad (59)$$

Where $C_{compr,op}$ is the operational compression cost, η_{compr} is the compressor efficiency and is assumed equal to 2.2 kWh/kgH_2 (Nguyen T., 2019), ν_{H2} represents the yearly hydrogen production.

$$C_{storage,OPEX} = 1\% \ C_{CAPEX} \ N_y \quad (60)$$

$$C_{AWE,OPEX} = 1\% \ C_{CAPEX} \ N_y \qquad (61)$$

$$C_{labor} = 5\% \ C_{CAPEX} \ N_y \ (62)$$

$$C_{compr,mant} = 4\% \ C_{CAPEX} \ N_y \ (63)$$

$$C_{el,mant} = 1\% \ C_{CAPEX} \ N_y \ (64)$$

The costs of maintaining the electrolyzer ($C_{AWE,OPEX}$), the hydrogen storage ($C_{storage,OPEX}$), the compressor ($C_{compr,mant}$), and the power grid ($C_{el,mant}$), as well as the cost of labor (C_{labor}), are determined as percentages of the CAPEX (Nguyen T., 2019).

By knowing each individual contribution of operating and maintenance costs, total OPEX costs can be obtained.

$$C_{OPEX} = \sum C_{OPEX,i} \quad (65)$$

$$C_{OPEX,y} = \frac{C_{OPEX}}{N_y} \quad (66)$$

The total cost of the plant thus amounts to:

$$C_{TOT} = C_{CAPEX} + C_{OPEX} \quad (67)$$

Finally, the investment and operational costs allow us to calculate the levelized cost of hydrogen (Nguyen T., 2019).

$$(LCoH_2)_{kg} = \frac{C_{CAPEX} \frac{i\,(i+1)^n}{(1+i)^n - 1} + C_{OPEX,y}}{\frac{W}{K}\, CF\ N_{hours,y}} \quad (68)$$

Where i is the rate of return, $C_{OPEX,y}$ is the yearly operational cost, K is the energy consumption of the electrolyzer, CF is the capacity factor and has a unit value as the electrolyzer works continuously.

It is also possible to find the levelized cost of hydrogen related to energy by dividing the value found in equation above by the *Lower Heating Value (LHV)* that is equal to 0.033 MWh/kg.

$$(LCoH_2)_{MWh} = \frac{(LCoH_2)_{kg}}{LHV} \quad (69)$$

4.3. Distillation and chromatography

The first experiments conducted in the laboratory of the Universidad Politécnica de Madrid concern the desalination of a synthetic marine water solution through three distillation processes in series to evaluate the rejection rate between distillations. The initial hypothesis is about the constant improvement of water quality as the number of serial distillations increased.

This study is necessary to assess the most appropriate number of serial distillations to achieve water salinity levels suitable for inclusion in the electrolyzer. This parameter is very important because it influences the high-performance lifetime of the electrolyzer. Specifically, the higher the salinity, the shorter the life cycle of the electrolyte with the consequent increase in risk and cost due to its replacement.

Firstly, a mixture of synthetic seawater with the salt concentrations in Table 1 is created to carry out the experiments. The salts used to create the synthetic marine water solution and carry out the laboratory experiments come from the *Panreac Química S.L.U.* company and are Sodium Chloride for molecular biology (NaCl) Magnesium Chloride 6-hydrate pure and pharma grade ($MgCl_2$ $6H_2O$), Calcium Chloride 6-hydrate for analysis ($CaCl_2$ $6H_2O$), Potassium Chloride pharma grade (KCl), Magnesium Sulfate 7-hydrate pure and pharma grade ($MgSO_4$ $7H_2O$), Sodium Hydrogen Carbonate pure and pharma grade ($NaHCO_3$) and Sodium Sulphate anhydrous for analysis (Na_2SO_4)

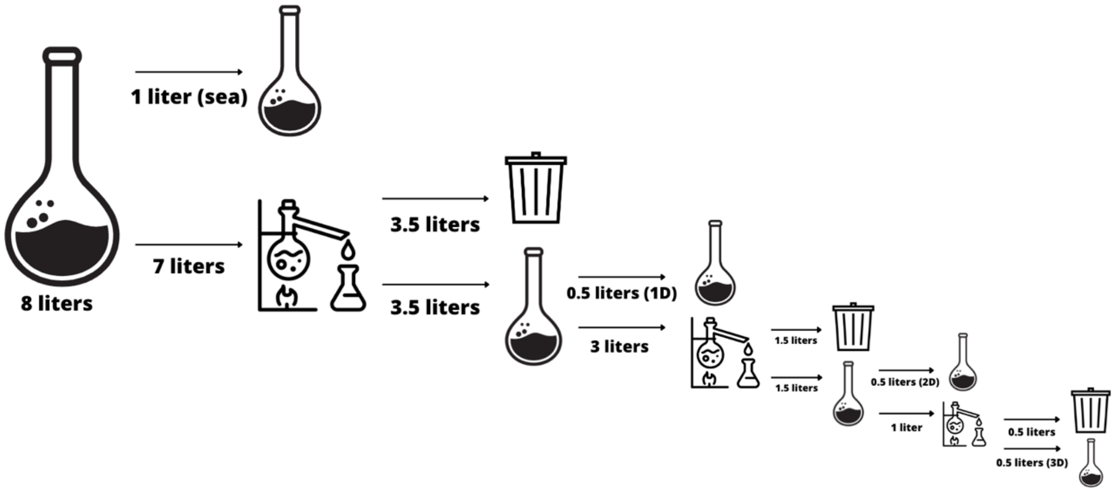

Figure 32: Sequential distillation synoptic diagram

As it is possible to see in the figure above, eight 1-liter solutions of distilled water are prepared to which the previously calculated amounts of salt are added until reaching a concentration of 35 grams of dissolved salts per liter of water.

Afterwards, seven liters of synthetic water are subjected to a first distillation while the remainder (1l) is stored for laboratory purpose. For each one-liter distillation, half of the processed amount is desalinated, while the remainder is discarded. A total of 3.5 liters of distilled water is then obtained from the first distillation, of which half a liter is kept for chromatography.

The remaining three liters are in turn subjected to a second distillation, from which 1.5 liters of distilled water is obtained. Again, half a liter is kept for laboratory analysis, while the remaining liter of water is returned to the distiller for a third distillation. From this last process half-liter of distilled water is obtained, which is stored for chromatography.

The figure below depicts the entire distillation system used in the laboratory including the distillation column inside which the water to be purified is contained, the heat exchanger that works in countercurrent and allows cooling of the steam produced by boiling water, the beaker, and the Agimatic-N heater stirrer.

Figure 33: Laboratory distillation system

The beaker, as well as the rest of the equipment, must be cleaned carefully as its function is to collect distilled water and it must not have any impurities that could alter the results.

The laboratory heater stirrer is characterized by a low power output (630 W) that greatly influences the duration of the experiment. In this case the distillation time for half a liter of water is equal to two and a half hours, of which half an hour is needed just to boil the water.

Initially, the measurements are taken with a salinity and conductivity meters, but they do not guarantee accurate precision because the post-distillation salinity levels are under the detection threshold of the laboratory equipment used.

Not having obtained the desired results using the laboratory's equipment and in search of more precise results, it is decided to contact a chemical analysis laboratory based in Tres Cantos and resort to chromatography. Specifically, ICP-OES chromatography is used, which is a process used to determine the concentration of several elements in the same sample and to trace the presence of metals in a solution. The atoms obtained by chromatography were Sodium (Na), Potassium (K), Magnesium (Mg), Calcium (Ca) and Sulphur (S).

This method is not useful to determine halogens or non-metals: for this reason, the concentrations of non-detected salts from this process are calculated through mathematical formulations.

Chromatography process consists of placing a sample in solution inside a high-temperature plasma in the form of a fine spray. The production of the plasma takes place in a flow of inert gas such as argon and is due to the presence of a high-intensity radio frequency energy field. The droplets are then vaporized and broken into their constituent parts. The atoms and ions produced emit light at different wavelengths that are measured by the process, which has a very high accuracy (Elga Veolia, 2021).

From the chromatography results, the relative error (δ_{rel}) of the concentration of synthetic seawater recreated in the laboratory compared to the ideal solution for each salt can be obtained as follows:

$$\delta_{rel} = \frac{c_{sea} - c_{isw}}{c_{sea}} \qquad (70)$$

Where c_{sea} is the concentration of the different salts of the synthetic seawater recreated in laboratory, and c_{isw} is the concentration of the different salts of the ideal synthetic seawater solution.

Afterwards, from the results obtained from the equation above the average (δ_{ave}) and the total relative error ($\delta_{rel,tot}$) can be calculated as follows:

$$\delta_{ave} = \frac{\Sigma\delta_i}{n_{salt}} \quad (71)$$

$$\delta_{rel,tot} = \frac{c_{sea,tot} - c_{isw,tot}}{c_{sea,tot}} \quad (72)$$

Where $c_{sea,tot}$ is defined as the sum of the concentrations of all salts relative to the laboratory-recreated mixture, while $c_{isw,tot}$ is defined as the sum of the concentrations of all salts in the ideal synthetic seawater solution.

Before continuing with the second part of the experiments, in which hydrogen is produced from desalinated synthetic seawater, it is necessary to know the mass of concentrated synthetic distilled water, pure water and caustic soda that make up the electrolyte. For each experiment, the proportions of the two water mixtures are changed to simulate the operation of the electrolyzer at different times.

To achieve this goal, the first values to be found are the molar concentrations per liter unit, which are obtained as follows:

$$x_i = \frac{c_i}{MM_i} \, (73)$$

Where c_i is the salt concentration of each ion after the first distillation and MM_i is the ion molar mass.

Then, the concentrations of ions not detected by chromatography (Cl^-, SO_4^{2-} and HCO_3^-) are determined by taking Sodium as the reference element using the following equation:

$$c_i = \frac{w_i}{w_{Na^+}} \, c_{Na} \, (74)$$

Where w_i is the concentration of an *i* salt before distillation.

Obtaining these values allows the calculation of the molar concentrations per unit liter of the non-detected ions by chromatography, which are determined with the equation above.

The next step is to calculate the molar concentrations per liter of the salts, which are calculated using the equations described on page 32. This makes it possible to calculate the mass concentrations (m_i) of each individual salt at the time of activation of the electrolyzer:

$$m_i = x_i \, MM_i \quad (75)$$

From these calculations, the total mass (m_{tot}) of each individual salt in the electrolyzer is then calculated:

$$m_{tot} = m_i \, V_{NaOH} \quad (76)$$

Where V_{NaOH} is the electrolyte volume, and it is considered equal to 11.08 m^3 as in the case study.

Using the previously obtained data it is possible to determine the number of salts present at different operation times (m_t):

$$m_t = \frac{(m_i \, N_{hours} \, \nu_{H2O} + m_{tot})}{V_{NaOH}} \quad (77)$$

Where N_{hours} is the number of operating hours, ν_{H2O} is the water consumption per hour and is equal to 348.48 kg/h as in the case study.

The mass in grams used as a reference for the preparation of the concentrated synthetic distilled water is that at 100,000 h because with the available instruments it is impossible to weigh masses of smaller orders of magnitude with high accuracy. $NaHCO_3$ is excluded from the weighing as it shows very small and therefore negligible concentrations.

Once this data is obtained, the mass of the concentrated synthetic distilled water for each selected operating time is calculated as follows:

$$m_{csdw} = \frac{m_{H2O} \, m_t}{m_{NaCl,100k}} \quad (78)$$

Where m_{csdw} is the concentrated synthetic distilled water mass, m_{H2O} is the total mass of water and is equal to 400 g and $m_{NaCl,100k}$ is the NaCl mass taken as reference at the operating time t = 100,000 hours. Finally, the mass of the distilled water (m_d) for each selected operating time can be evaluated:

$$m_d = m_{H2O} - m_{csdw} \quad (79)$$

4.4. Cell design and construction

The electrolysis cell was designed with 3D modelling software called Rhinoceros and printed with a 3D printer Ultimaker using two different materials: Polylactic Acid (PLA) and Polypropylene (PP).

The design of the two cells with materials with different physical and chemical properties allowed the comparison of their different behavior in contact with a strong mineral base, such as NaOH.

Once the various components of the cell were printed, for practical reasons it is convenient to use a cutter to remove the parts that are not useful for the construction of the cell, i.e., those that join the four parts together at the output of the 3D printer.

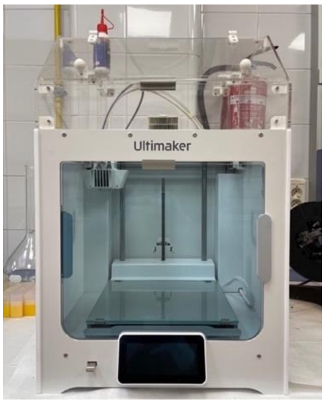

Figure 34: Ultimaker Laboratory 3D printer

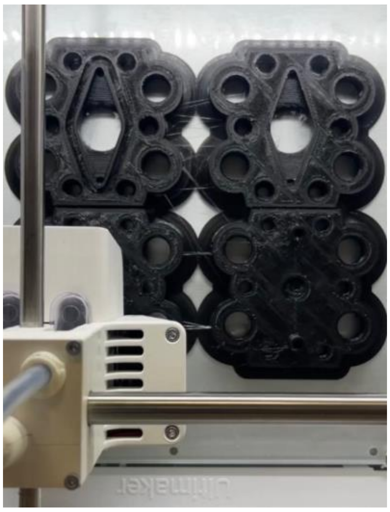

Figure 35: 3D printer during PLA cell printing

After separating the four components of the cell, these are placed inside an aqueous solution at room temperature for all the PVA to dissolve. To achieve a good result, the various components of the cell can be left inside a tank filled with water on any surface or above a magnetic stirrer.

The dissolution times are very different and in the second case are dramatically reduced as the stirrer aids the process through a continuous motion of the water generated by the magnetic interaction of the device's surface with a previously inserted magnet. For laboratory purposes, the Agimatic-N stirrer shown in Figure 33 was used. Afterwards, the cell components are washed more thoroughly with running water to remove any further traces of PVA.

Printing the cell is very time consuming as it can take up to 48 hours, so in the meantime you can proceed to print other components such as the photopolymer resin sealing rings. These are molded with a resin printer and before they are used, they must be placed inside an ultrasonic bath so that all impurities are removed.

This process is widely used in the medical, laboratory and electronic fields as it is very effective on different types of elements. The technology consists of the generation of ultrasonic vibrations in the water that give rise to the formation of vacuum bubbles that instantly implode and thoroughly clean the objects inside.

Figure 36: Laboratory ultrasonic bath

Subsequently, the sealing rings are inserted in the gasket grooves of the cell to prevent electrolyte leakage during operation as depicted in Figure 37.

The next step is to thread the hole into which the banana plug will be placed with a tap wrench to achieve a perfect fit. After that, assembly of the cell can begin with the insertion of the gold banana plugs into the middle and outer parts of the two outer plates and the addition of the electrodes into the square cavities on the inner part of the same plates.

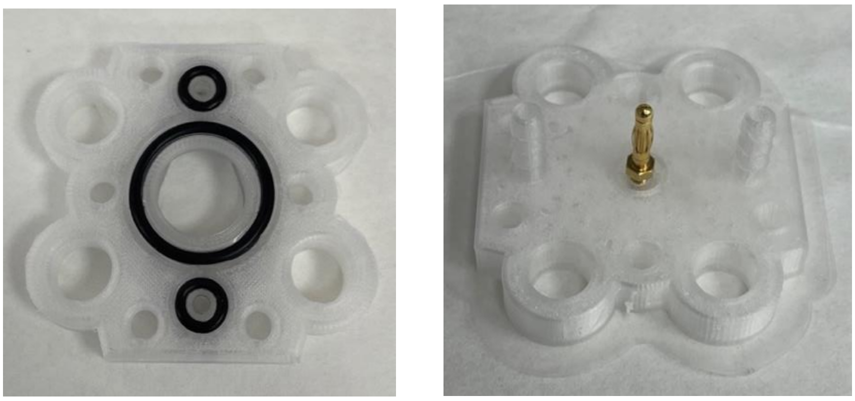

Figure 37: Insertion of the sealing rings and banana into the cell plug after threading

The electrode is composed of 316l stainless steel foil, and prior to placement inside the plates, it must be shaped so that there are no gaps in the cavity that would generate electrolyte leakage. This process is carried out by means of a rough surface, which makes it possible to obtain through a rubbing operation a suitably sized piece.

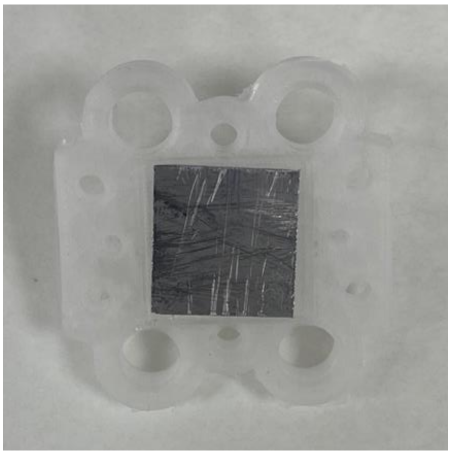

Figure 38: Insertion of the electrodes

Next, all six screws are inserted, which are tightened by means of screwdrivers using the wrench and counter wrench method. The screws are tightened in "crisscross" passes, using the star method, to equalize the torque over the entire contact area and avoid tightening predominantly on one side.

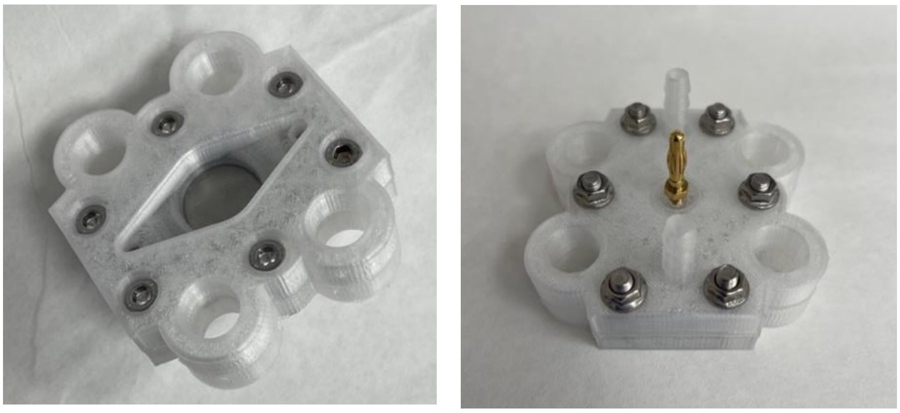

Figure 39: Insertion of the small screws

At the end of this procedure, a conductivity meter is used to verify that the electrode is in contact with the corresponding banana plug and that there is therefore an electrical connection that allows a voltage difference to be applied when hydrogen is to be produced. Obtaining non-zero resistance values assures that both components are placed correctly in the cell and allows to proceed with the next steps.

The two pieces are then joined together by four larger screws using the same procedure as previously used with the small screws.

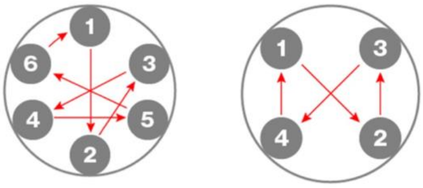

Figure 40: Screwing star method (La Gazzetta dello Sport, 2023)

Figure 41: Laboratory-built electrolyzer cell

The cell depicted in Figure 41 is then ready to be connected to the system for hydrogen production.

The characteristic parameters of our cell are:

$$j = 300 \frac{mA}{cm^2} = 0.3 \frac{A}{cm^2} \; (80)$$

$$d_{lab} = 2 \; cm \; (81)$$

where j is the current density and d represents the distance between the two electrodes.

From these initial data, it is possible to evaluate the value of the area of the cell (A) and the current flowing through the cell (I):

$$A_{lab} = \frac{\pi d^2}{4} = 3.14 \; cm^2 \; (82)$$

$$I = jA = 0.94 \; A \; (83)$$

Then, a voltage value equal to 1.8 V is assumed and the electric power consumed by the cell is calculated.

$$W = VI = 2 \; W \; (84)$$

After that, it was possible to determine the hydrogen production rate as follow:

$$\mathcal{V}_{H_2} = \frac{\eta_F n_c I}{zF} = 0.394 \frac{mol}{s} \; (85)$$

Where η_F is the Faraday efficiency considered constant and equal to 0.999, and n_c is the number of cells connected in series. In this case we refer to only one cell, so n_c has unit value.

4.5. Laboratory hydrogen production

The second part of the experiments concerns the production of hydrogen with the alkaline polypropylene electrolyzer, designed and built in the laboratory.

Firstly, the cell is connected to the electrolyte storage tank via *R.S. 293-2000 polyvinyl chloride (PVC)* tubing and to a power supply by inserting the two direct current source wire sockets on the cell's gold banana plugs. Afterwards, a thermometer is placed inside the electrolyte container to check its temperature during operation.

After connecting the whole system, the electrolyte consisting of 80% by weight water and the remaining 20% caustic soda is prepared. More specifically mixtures of 500g consisting of 100g caustic soda and 400g water are prepared to perform the experiments.

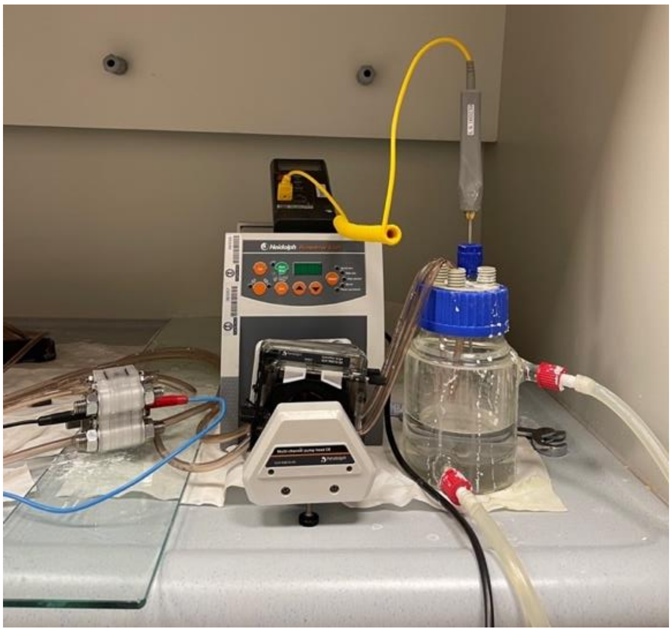

Figure 42: Test bench

The caustic soda is initially weighed using the laboratory *A&D EK-6000G* balance and then placed in a small where the mixture of distilled water and concentrated synthetic distilled water is added.

To facilitate the dissolution of the caustic soda and to prevent it from sticking to the bottom, the mixture is carefully stirred with a small spoon. In a very few seconds, the mixture reaches very high temperatures due to the reaction of sodium hydroxide with water, that makes its transport difficult. So, it is necessary to wait about thirty minutes for the mixture to cool down before inserting the electrolyte into the storage tank.

The handling of caustic soda is done with care and utmost caution, as it is a corrosive material and can cause harm to people or the environment. All equipment available in the laboratory is used, such as plastic gloves, apron, and goggles, to avoid severe skin burns and permanent stains on clothes.

When the electrolyte is well dissolved and at room temperature, half of it is placed inside the inner chamber of the electrolyte storage tank and circulated by activating the peristaltic pump to purge the tubes.

Afterwards, the other half of the electrolyte is inserted. Heat exchange by conduction allows the temperature of the electrolyte to be raised to the operation temperature of 60°C. It is heated by means of a thermostatic bath set at a temperature of 83°C, which send water inside the external chamber of the electrolyte tank by means of the J.P. Selecta laboratory pump.

Figure 43: Laboratory thermostatic bath and J.P Selecta pump

This pump is switched on when the temperature of the electrolyte is falling below the operating temperature, while it is switched off in the case of an excessive rise in temperature.

When the operating temperature is reached, the electrolyte is pumped inside the cell by means of the *Heidolph Pumpdrive 5201* peristaltic pump in Figure 44 operating at a shaft rotation speed of 60 rpm. As well, the programmable direct current power supply SIGLENT SPD3303X-E is turned on to start producing hydrogen and to carry out the experiments at constant current.

Figure 44: Laboratory peristaltic pump and power supply

To calculate the current at which to carry out the experiments, eleven current density values characteristics of commercial alkaline electrolyzers is arbitrarily selected. For each current value, a voltage value is found using a voltmeter.

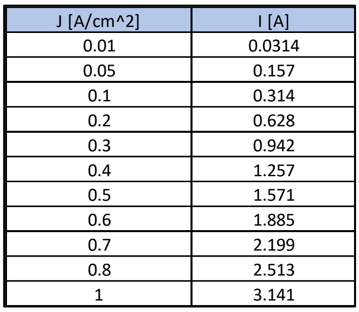

J [A/cm^2]	I [A]
0.01	0.0314
0.05	0.157
0.1	0.314
0.2	0.628
0.3	0.942
0.4	1.257
0.5	1.571
0.6	1.885
0.7	2.199
0.8	2.513
1	3.141

Table 8: Current density used to conduct experiments

The experiment is repeated ten times and each one is characterized by an aqueous solution with different concentrations of synthetic distilled water to simulate the operation of the electrolyzer at different times. In particular, the voltage was evaluated at different current intensities at 0 h, 1,000 h, 2,000 h, 3,000 h, 4,000 h, 5,000 h, 10,000 h, 25,000 h, 50,000 h, 100,000 h after activation of the electrolyzer.

In this analysis, it is assumed that during electrolyzer operation, impurities remain within the electrolyte while water is consumed to produce hydrogen. Through these experiments, it is possible to determine the polarization curves and evaluate the increase in voltage as the hours of operation increase. In particular, the loss of electrolyzer efficiency over time due to electrolyte degradation caused by the use of desalinated saltwater instead of freshwater is analyzed.

4.6. Additional cost of electrolyte management

The additional cost of the electrolyte management (C_{EM}) results from using desalinated saltwater instead of freshwater in the alkaline electrolyzer. In this analysis, it is assumed that deterioration due to the increasing presence of impurities over time causes an increase in cell voltage and a substantial loss of performance causing an increase of the total costs of the electrolyzer.

This additional cost is due to the presence of dissolved species in seawater and can be described as the combination of the renewal of the electrolyte (C_{NaOH}) that needs to be done during the life cycle and the energy losses (C_{eled}) due to the additional resistance of the deteriorated electrolyte.

The electrolyte management cost is calculated as follows:

$$C_{EM} = C_{eled} + C_{NaoH} \quad (86)$$

Where C_{eled} is defined as:

$$C_{eled} = c_{el} E_{eled} \frac{T_{LC}}{T_{ER}} \quad (87)$$

Where c_{el} is the electricity cost of the case study, T_{LC} is the life cycle of the electrolyzer and T_{ER} is the electrolyte renewal time, E_{eled} represent the induced energy losses due to electrolyte degradation and is defined as:

$$E_{eled} = \int_0^{T_{ER}} \Delta R(t) I^2 \, dt \quad (88)$$

On the other hand, the electrolyte renewal cost can be defined as:

$$C_{NaOH} = c_{NaOH} \frac{T_{LC}}{T_{ER}} \quad (89)$$

Where c_{NaOH} is the electrolyte renewal cost of the case study.

By substituting the equations of C_{NaOH} and C_{eled} the relation that must be minimized for optimization is obtained:

$$C_{EM} = (c_{el} \int_0^{T_{ER}} \Delta R(t) I^2 \, dt + c_{NaOH}) \frac{T_{LC}}{T_{ER}} \quad (90)$$

However, the first step in determining the additional cost of the electrolyte management is to estimate the laboratory resistance (ΔR_{lab}) and the resistivity ($\Delta \rho_{lab}$) variation values from the voltage values obtained during hydrogen production. The aim of the following calculations is to check which trend best fits the resistance variation data over time of the case study to obtain numerical results concerning the management cost the electrolyte.

$$\Delta R_{lab} = \frac{\Delta V}{I_{lab}} \quad (91)$$

Where ΔV represents the voltage variation between two instants of time, I_{lab} is the current flowing through the laboratory cell.

$$\Delta \rho_{lab} = \Delta R_{lab} \frac{A_{lab}}{d_{lab}} \quad (92)$$

Where A_{lab} and d_{lab} are the area and the distance between the electrodes of the laboratory cell, $\Delta \rho_{lab}$ is the variation in resistivity over time and is equal to $\Delta \rho_{cs}$ because this parameter depends only on the operating temperature.

Once obtained the resistivity value of the case study, it is then possible to proceed with the calculation of the resistance variation of the case study (ΔR_{cs}).

$$\Delta R_{cs} = \Delta \rho_{cs} \frac{d_{cs}}{A_{stack}} N_c \quad (93)$$

Where A_{stack} and d_{cs} are the area and the distance between the electrodes of the case study cell.

Afterwards, the trend equation best suited to our data set was determined by comparing various trends on Excel, which is the following:

$$\Delta R = A \ln(t) + b \quad (94)$$

Then, it is necessary to determine the percentage error relative to the constants (A, b) to assess whether and how much it impacts the results. Knowing the results of the linear regression related to the error of the two constants this parameter can be found as follows:

$$Err_{A\%} = \frac{Err_A}{A} \quad (95)$$

$$Err_{b\%} = \frac{Err_b}{b} \quad (96)$$

Finally, to verify that the error does not propagate within these equations, all possible combinations considering the limit values of the constants A and b are evaluated as follows:

$$A_{max} = A + Err_A \quad (97)$$

$$A_{min} = A - Err_A \quad (98)$$

$$b_{max} = b + Err_b \quad (99)$$

$$b_{min} = b - Err_b \quad (100)$$

5. Results and Discussion

This chapter shows all the numerical results obtained from carrying out the methodologies of the previous chapter. In particular, the results obtained from the economic evaluation of the alkaline electrolyser in the case study, chromatography, hydrogen production in the laboratory and the additional cost due to the electrolyte management are described and commented on.

5.1. Results of the economic evaluation of the case study

The following tables summarize the results concerning the absolute fixed costs, the indirect costs, and the operational and maintenance costs:

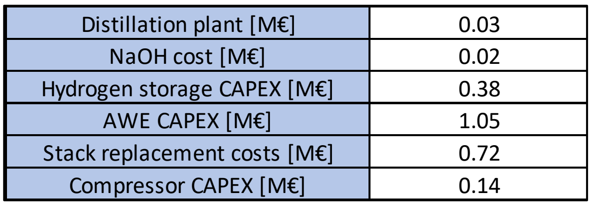

Distillation plant [M€]	0.03
NaOH cost [M€]	0.02
Hydrogen storage CAPEX [M€]	0.38
AWE CAPEX [M€]	1.05
Stack replacement costs [M€]	0.72
Compressor CAPEX [M€]	0.14

Table 9: Plant absolute fixed costs

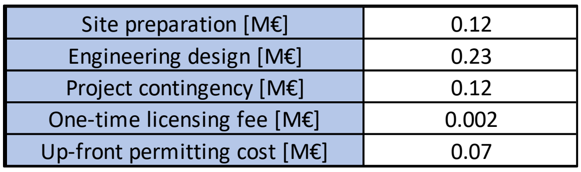

Site preparation [M€]	0.12
Engineering design [M€]	0.23
Project contingency [M€]	0.12
One-time licensing fee [M€]	0.002
Up-front permitting cost [M€]	0.07

Table 10: Plant indirect costs

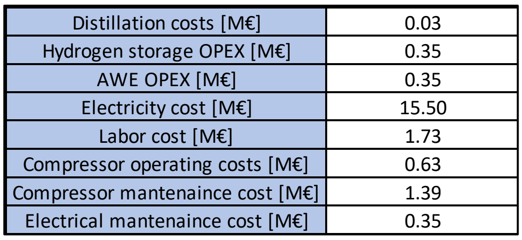

Distillation costs [M€]	0.03
Hydrogen storage OPEX [M€]	0.35
AWE OPEX [M€]	0.35
Electricity cost [M€]	15.50
Labor cost [M€]	1.73
Compressor operating costs [M€]	0.63
Compressor mantenaince cost [M€]	1.39
Electrical mantenaince cost [M€]	0.35

Table 11: Plant operational and maintenance costs

The table below shows the results of the CAPEX and OPEX costs and the total plant costs:

C_{fixed} [M€]	2.35
$C_{indirect}$ [M€]	0.54
C_{CAPEX} [M€]	2.89
$C_{CAPEX,y}$ [M€/y]	0.24
C_{OPEX} [M€]	20.31
$C_{OPEX,y}$ [M€/y]	1.69
C_{TOT} [M€]	23.20
$C_{TOT,y}$ [M€/y]	1.93

Table 12: CAPEX, OPEX and total plant costs

Figure 45 and Table 13 provide qualitative and quantitative data of the relative weight of each individual cost to understand which is the most economically impactful.

Distillation plant [M€]	0.13%
NaOH cost [M€]	0.10%
Hydrogen storage CAPEX [M€]	1.65%
AWE CAPEX [M€]	4.54%
Stack replacement costs	3.09%
Compressor CAPEX [M€]	0.60%
Site preparation [M€]	0.51%
Engineering design [M€]	1.01%
Project contingency [M€]	0.51%
One-time licensing fee [M€]	0.01%
Up-front permitting cost [M€]	0.30%
Distillation costs [M€]	0.12%
Hydrogen storage OPEX [M€]	1.49%
AWE OPEX [M€]	1.49%
Electricity cost [M€]	66.81%
Labor cost [M€]	7.47%
Compressor operating costs [M€]	2.70%
Compressor mantenaince cost [M€]	5.98%
Electrical mantenaince cost [M€]	1.49%

Table 13: Weight of each cost in relation to total cost

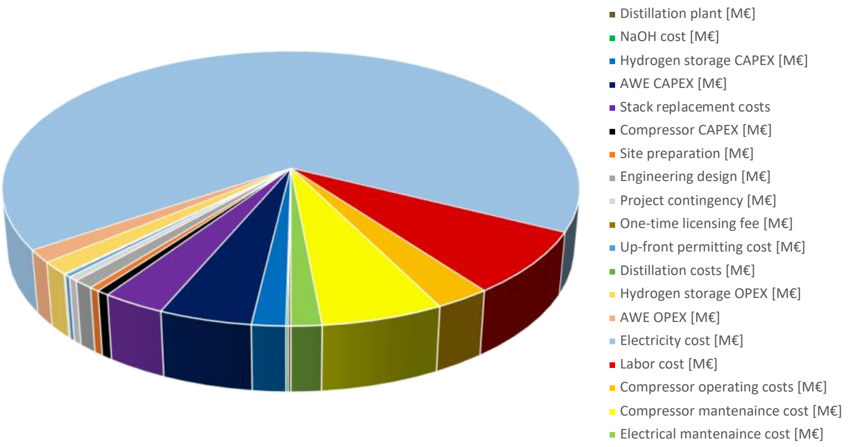

Figure 45: Costs pie chart

Finally, the calculation of the total cost of the installation allows the calculation of the levelized cost of hydrogen:

LCoH [€/kg]	6.25
LCoH [€/MWh]	187.70

Table 14: Levelized cost of hydrogen

The levelized cost value of hydrogen is slightly higher than the range of values found in the literature (1.6-5 $/kg) due to the recent increase in the cost of electricity, which causes a significant increase in hydrogen compression and electrolysis costs. The distillation plant and desalination operating costs also contribute, albeit to a small extent. However, in the future, the foreseeable increase in energy production from renewable sources, as well as energy efficiency and reduced dependence on fossil fuels, could ensure much lower electricity costs.

In addition, the alkaline electrolyser CAPEX, the stack replacement costs, and the compressor maintenance costs still represent a large percentage of the total. However, these costs could be reduced in the future by the increase in energy demand for hydrogen and the development of more advanced and efficient technologies.

5.2. Chromatography and distillation results

The Table 15 summarizes the results obtained from chromatography: the label c_{sea} indicates the pre-distillation salt concentration values, while c_{1D}, c_{2D}, c_{3D} represent the data after the first, second and third distillation, respectively.

Atoms	c_{sea} [mg/l]	c_{1D} [mg/l]	c_{2D} [mg/l]	c_{3D} [mg/l]
Na	9,600	0.15	<0.10	<0.10
K	492	0.08	0.06	0.10
Mg	1,450	<0.05	<0.05	<0.05
Ca	550	<0.05	<0.05	<0.05
S	760	<0.05	<0.05	<0.05

Table 15: Chromatography results

From the chromatography results, it can be noted that this inexpensive and easily applied process is very efficient because the difference in salt concentration before and after the distillation processes is enormous. In addition, these results also show that the initial hypothesis is incorrect, as the salt content reaches a horizontal asymptote after the first distillation.

The obtained results suggest that one distillation is the right trade-off between reducing salinity and increasing costs due to desalination because the only significant reduction in the concentration of salts between the first and second distillations concerns the sodium atom. The others (K, Mg, Ca, S) remain almost constant.

From this analysis, it is finally concluded that if it were necessary to reduce salinity values again after the first distillation, one should change the process and use more efficient deionization processes such as electrodialysis because a series of consecutive distillations causes only an increase in cost without a substantial increase in benefit.

It is also important to comment on the concentration of potassium, which drops steeply after the first distillation, continues to drop following the second distillation, but rises slightly at the end of the third process. The rise is probably due to residual salt at the bottom of the distiller that remained despite thorough cleaning of the distillation system or to an error due to chromatography uncertainty. It is certainly not possible for the salinity value to rise following a distillation.

Finally, an error in the salinity measurement before the first distillation probably due to a lack of precision of the balance present in the laboratory and/or a tolerance present in the chromatography must be pointed out. The difference between the ideal and the real values are tabulated in the table below:

Atoms	C_{sea} [mg/l]	C_{isw} [mg/l]
Na	9,600	10,742
K	492	399
Mg	1,450	1,283
Ca	550	412
S	760	905

Table 16: Difference between ideal and real values obtained by chromatography

From these values, the relative error (δ_{rel}) for each salt can be obtained:

Atoms	Relative error [%]
Na	11.90
K	18.90
Mg	11.52
Ca	25.09
S	19.08
Total	6.92

Table 17: Relative error of the measurements

Therefore, the average error (δ_{ave}) is equal to:

$$\delta_{ave} = 17.3\ \% \qquad (101)$$

From Table 17, it can be noted that the relative error of some measurements related to the individual salt is quite high as in the case of *Calcium, Sulfur, or Potassium*. Despite of this, out of the total this percentage is dramatically reduced:

$$\delta_{rel,tot} = 6.92\ \% \ (102)$$

The decision not to carry out serial distillations and therefore to perform only one distillation allows all the following calculations to be performed with the chromatography results referring to the first distillation. For the elements such as *Magnesium, Calcium* and *Sulphur* that are characterized by concentration values below 0.05%, the largest value is taken into account in the calculations to be conservative.

The table below contains the molar concentrations per liter unit of both the detected and non-detected ions:

Solute	c_{1D} [mg/L]	x [mol/L]
Na^+	0.15	6.52E-06
Mg^{2+}	0.05	2.06E-06
Ca^{2+}	0.05	1.25E-06
K^+	0.08	2.05E-06
Cl^-	0.269	7.59E-06
SO_4^{2-}	0.038	3.93E-07
HCO_3^-	0.00146	2.39E-08

Table 18: Calculation of the number of moles per liter of each ion

From the values above, the mass concentrations and the total masses of each salt at the instant of activation of the electrolyzer are calculated. The values are summarized in the Table 19 and in the Table 20:

Salt molecules	x [mol/l]	MM [g/mol]	m [g/l]
NaCl	6.50E-06	58.443	3.80E-04
$MgCl_2$	2.06E-06	203.3	4.18E-04
$CaCl_2$	1.25E-06	219.09	2.73E-04
KCl	2.05E-06	74.55	1.53E-04
$MgSO_4$	3.93E-07	246.48	9.68E-04
$NaHCO_3$	2.39E-08	84.01	2.01E-06

Table 19: Calculation of the mass of salt per liter of solution

Salt molecules	m_{tot} [g]
NaCl	4.21
$MgCl_2$	4.63
$CaCl_2$	3.03
KCl	1.69
$MgSO_4$	1.07
$NaHCO_3$	0.022

Table 20: Total mass of salts at the time of activation of the electrolyzer

Finally, all the salt mass data at different time instants are calculated using the equation on page 64, and are collected in Table 21 and Table 22.

[hours]	0	1,000	2,000	3,000	4,000	5,000
NaCl [g]	3.80E-04	1.23E-02	2.43E-02	3.62E-02	4.82E-02	6.01E-02
$MgCl_2$ [g]	4.18E-04	1.36E-02	2.67E-02	3.99E-02	5.30E-02	6.62E-02
$CaCl_2$ [g]	2.52E-03	8.87E-03	1.75E-02	2.61E-02	3.47E-02	4.33E-02
KCl [g]	1.53E-04	4.95E-03	9.75E-03	1.45E-02	1.93E-02	2.41E-02
$MgSO_4$ [g]	9.68E-05	3.14E-03	6.19E-03	9.23E-03	1.23E-02	1.53E-02
$NaHCO_3$ [g]	2.01E-06	6.51E-05	1.28E-04	1.91E-04	2.55E-04	3.18E-04

Table 21: Increase in salt concentration from 0 to 5,000 hours

[hours]	10,000	25,000	50,000	100,000
NaCl [g]	1.20E-01	2.99E-01	5.98E-01	1.20
$MgCl_2$ [g]	1.32E-01	3.29E-01	6.58E-01	1.32
$CaCl_2$ [g]	8.62E-02	2.15E-01	4.30E-01	8.60E-01
KCl [g]	4.81E-02	1.20E-01	2.40E-01	4.80E-01
$MgSO_4$ [g]	3.05E-02	7.62E-02	1.52E-01	3.05E-01
$NaHCO_3$ [g]	6.33E-04	1.58E-03	3.16E-03	6.32E-03

Table 22: Increase in salt concentration from 10,000 to 100,000 hours

Therefore, the following proportions of concentrated synthetic distilled water and pure water are found:

[hours]	0	1,000	2,000	3,000	4,000	5,000
Concentrated synthetic distilled water [g]	0.13	4.11	8.10	12.09	16.08	20.06
Pure water [g]	399.87	395.88	391.90	397.91	383.92	379.94

Table 23: Mixture composition from 0 to 5,000 hours

[hours]	10,000	25,000	50,000	100,000
Concentrated synthetic distilled water [g]	40	99.81	199.49	398.86
Pure water [g]	360	300.19	200.51	1.14

Table 24: Mixture composition from 10,000 to 100,000 hours

5.3. Hydrogen production results

Table 25 and Figure 46 depict the quantitative and qualitative increase in voltage with increasing hours of operation, respectively.

J [A/cm^2]	I [A]	V1000 [V]	V2000 [V]	V3000 [V]	V4000 [V]	V5000 [V]
0.01	0.0314	1.839	1.84	1.842	1.85	1.852
0.05	0.157	2.077	2.081	2.083	2.101	2.124
0.1	0.314	2.29	2.294	2.31	2.33	2.335
0.2	0.628	2.643	2.662	2.674	2.677	2.677
0.3	0.942	3.032	3.033	3.073	3.081	3.082
0.4	1.256	3.381	3.412	3.432	3.442	3.451
0.5	1.570	3.732	3.771	3.788	3.801	3.81
0.6	1.884	4.101	4.139	4.146	4.149	4.154
0.7	2.199	4.465	4.467	4.491	4.506	4.522
0.8	2.513	4.8	4.843	4.861	4.873	4.888
1	3.141	5.557	5.59	5.603	5.622	5.659

Table 25: Polarization curves at different operating times (0h-5,000h)

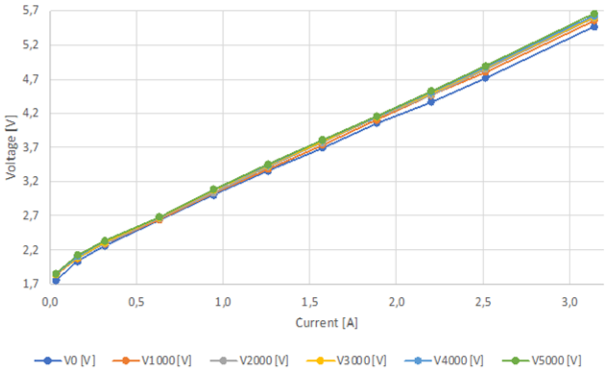

Figure 46: Polarization curves at different operating times (0h-5,000h)

These results are consistent with what was expected because the greater the circulation of electrolyte, the greater the number of impurities remaining within the electrolyzer. However, as can be seen in Figure 46, considering the range from 0 to 5,000 hours, the voltage difference at the same current density is not excessively large.

For this reason, it is decided to evaluate higher values of operating hours until a limit value of 100,000 h is reached. From Table 26 and Figure 47, an appreciable change in voltage can be seen in a quantitative and qualitative manner.

J [A/cm^2]	I [A]	V0 [V]	V1000 [V]	V5000 [V]	V10000 [V]	V50000 [V]	V100000 [V]
0.01	0.0314	1.753	1.839	1.852	1.853	1.858	1.86
0.05	0.157	2.033	2.077	2.124	2.142	2.1	2.113
0.1	0.314	2.26	2.29	2.335	2.366	2.336	2.339
0.2	0.628	2.635	2.643	2.677	2.75	2.721	2.745
0.3	0.942	3.001	3.032	3.082	3.101	3.169	3.192
0.4	1.256	3.356	3.381	3.451	3.461	3.553	3.562
0.5	1.570	3.69	3.732	3.81	3.82	3.855	3.906
0.6	1.884	4.053	4.101	4.154	4.165	4.232	4.293
0.7	2.199	4.36	4.465	4.522	4.544	4.56	4.627
0.8	2.513	4.712	4.8	4.888	4.891	4.955	5.06
1	3.141	5.466	5.557	5.659	5.68	5.692	5.743

Table 26: Polarization curves at different operating times (0h-100,000h)

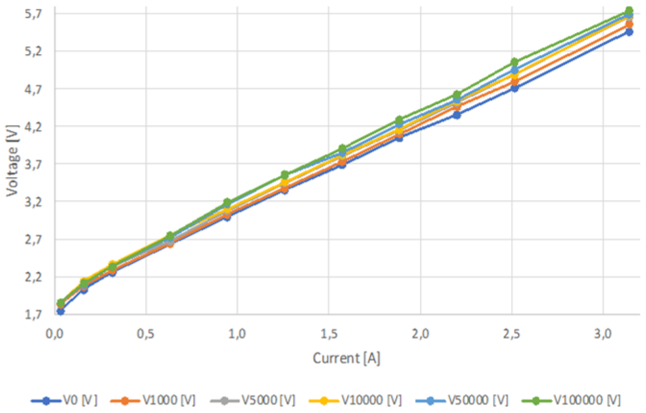

Figure 47: Polarization curve at different operating time (0h-100,000h)

5.4. Additional costs of electrolyte management results

In Table 27, all data from the previous analysis are collected at this current density with the aim of evaluating the trend of voltage as the hours of operation change.

Hours [h]	V [V]	V Nc [V]
0	3.001	597.20
1,000	3.032	603.37
2,000	3.033	603.57
3,000	3.073	611.53
4,000	3.081	613.12
5,000	3.082	613.32
10,000	3.101	617.10
25,000	3.134	623.67
50,000	3.169	630.63
100,000	3.192	635.21

Table 27: Voltage variation with varying operating hours

at a defined current density of 300 mA/cm²

Initially, the first 4,000 hours of operation are plotted to investigate the evolution of voltage with respect to time. As it is possible to see in Figure 48 the trend is linear and the inaccuracies from the ideal linear trend are only due to the accuracy of the voltmeter used to determine the voltage. This trend confirms the PhD results obtained by D'Amore-Domenech (2021).

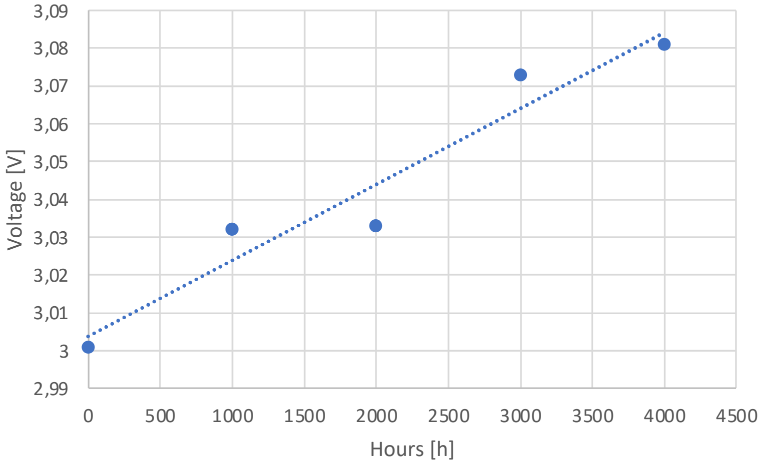

Figure 48: Voltage evolution from 0 to 4,000 hours with linear trend line

Afterwards, the entire operating range of the alkaline electrolyzer is analyzed. For the first time in the available literature the results in Figure 49 show a non-linear trend and for this reason an analysis on the trend line that best fit these data is done.

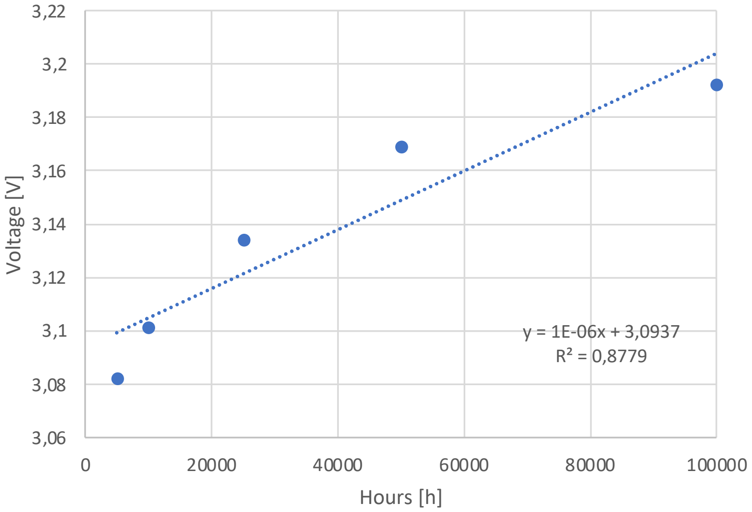

Figure 49: Voltage evolution from 0 to 100,000 hours with linear trend line

The potential, logarithmic, polynomial, and exponential trend are analyzed but the two that best represent the trend are the first two. However, the potential trend is chosen as it is the most accurate due to the higher value of R^2 which can be observed in Figure 50 and Figure 51. More specifically, the closer this value is to unity, the more precise the trend line under assessment.

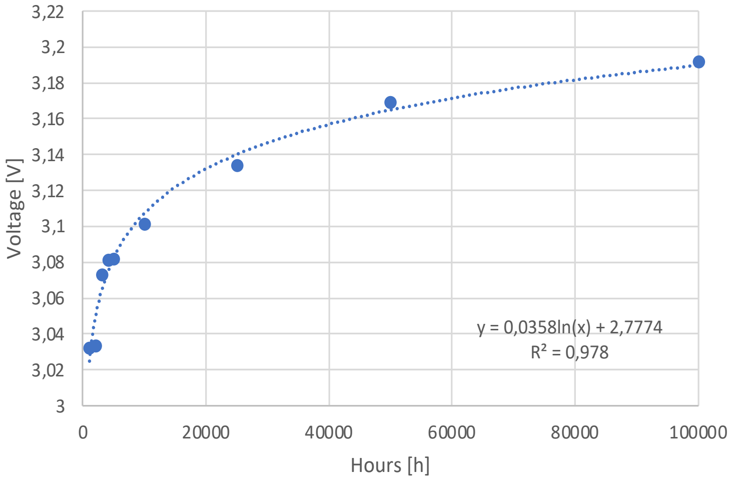

Figure 50: Voltage evolution from 0 to 100,000 hours with logarithmic trend line

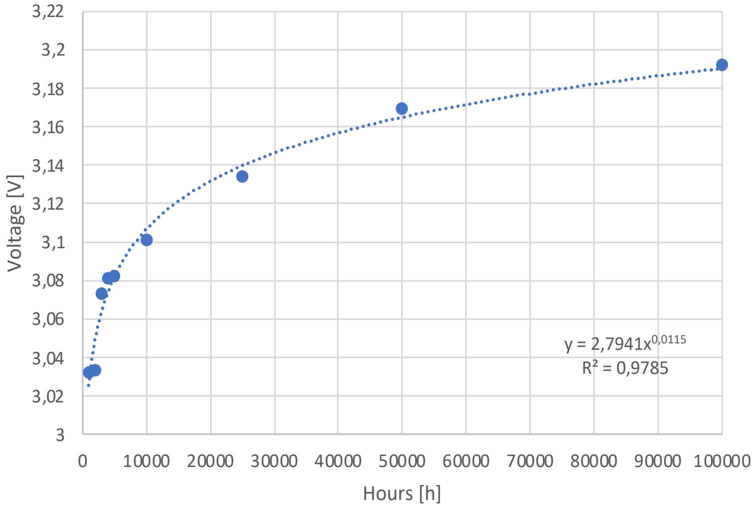

Figure 51: Voltage evolution from 0 to 100,000 hours with potential trend line

The table below collects all resistance and resistivity variation values for the laboratory case and the case study:

Hours [h]	V [V]	ΔR_{lab} [Ohm]	$\Delta \rho_{lab}$ [Ohm m]	ΔR_{cs} [Ohm]
0	3.001	0	0	0
1,000	3.032	0.033	0.052	0.00044
2,000	3.033	0.034	0.053	0.00045
3,000	3.073	0.077	0.120	0.00102
4,000	3.081	0.085	0.134	0.00113
5,000	3.082	0.086	0.135	0.00115
10,000	3.101	0.106	0.167	0.00141
25,000	3.134	0.141	0.222	0.00189
50,000	3.169	0.178	0.281	0.00238
100,000	3.192	0.203	0.319	0.00271

Table 28: Resistance values and changes in resistance as the hours change

As can be noted in Figure 52, the trend of the resistance change related to the case study versus the device's operating hours is logarithmic and is described by the following equation:

$$\Delta R = A\ ln(t) + b\ (103)$$

Where A and b are two constants, h the operating hours and ΔR the resistance variation.

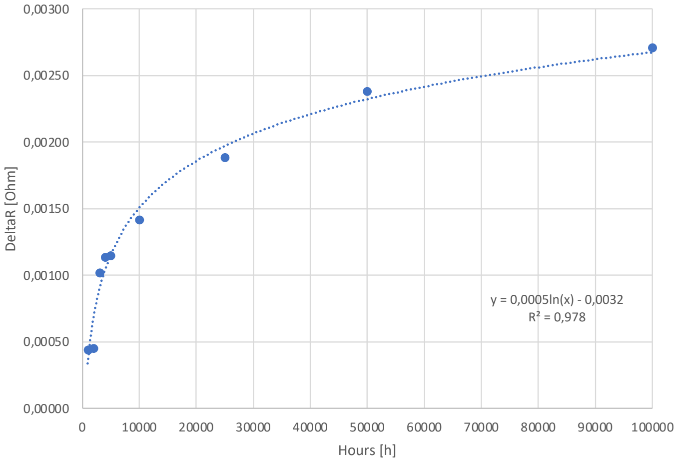

Figure 52: Evolution of the resistance variation with respect to the operating hours

The trend of the ΔR function over time can then be substituted within the equation $E_{eled} = \int_0^{T_{ER}} \Delta R(t) I^2 \, dt$ (88):

$$E_{eled} = \int_0^{T_{ER}} A I^2 \ln(T_{ER}) + b I^2 \, dt \quad (104)$$

The result of the integral in the time interval of interest is equal to:

$$E_{eled} = A I^2 (T_{ER} \ln(T_{ER}) - T_{ER}) + b I^2 \, T_{ER} \quad (105)$$

Therefore:

$$C_{EM} = [(c_{el} A I^2 (T_{ER} \ln(T_{ER}) - T_{ER}) + c_{el} b I^2 \, T_{ER}) + c_{NaOH}] \frac{T_{LC}}{T_{ER}} \quad (106)$$

Calculating the derivative of the function and setting it to zero yields the minimum of the function, which corresponds to the lowest cost of managing the electrolyte:

$$\frac{dc_{EM}}{dT_{ER}} = \frac{c_{el} \, A I^2}{T_{ER}} - \frac{c_{NaOH}}{T_{ER}^2} = 0 \quad (107)$$

Therefore:

$$T_{ER} = \frac{c_{NaOH}}{A I^2 \, c_{el}} = 20{,}026 \, h \quad (108)$$

This is an interesting result as it turns out that the alkaline electrolyte is economically efficient for one fifth of the operating hours of the electrolyzer. It is therefore only necessary to change the electrolyte five times during the entire life cycle.

By substituting this value into the above equations, the following results can be found:

$$E_{eled} = 760\ MWh$$

$$c_{EM} = 0.4\ M\text{€}$$

Considering the hydrogen production of the case study electrolyzer equal to 4,070,244 kg during its entire life cycle, the additional cost of each electrolyte replacement per kg of hydrogen can be determined:

$$c_{add_{electrolyte}} = \frac{c_{EM}}{v_{H_2} N_y} = 0.09 \frac{\text{€}}{kg} \quad (109)$$

Finally, the results of the linear regression are summarized in the table below:

A [Ohm]	5.08E-04
Err_A [Ohm]	2.88E-05
$\%err_A$	5.67%

b [Ohm]	-3.17E-03
Err_b [Ohm]	2.62E-04
$\%err_b$	-8.27%

Table 29: Linear regression results

Therefore:

A_{max}	5.37E-04
A_{min}	4.79E-04

b_{max}	-2.91E-03
b_{min}	-3.43E-03

Table 30: Maximum and minimum error of the constants

The different combinations of the constants reveal the following results:

	A_{max},b_{min}	A_{max},b_{max}	A_{min},b_{min}	A_{min},b_{max}
T_{ER} [h]	18,951	18,951	21,229	21,229
E_{ELED} [MWh]	700	980	513	826
C_{EM} [M€]	0.4	0.5	0.3	0.4

Table 31: Evaluation of the error propagation

From these results, it can be stated that the renewal time of the electrolyte does not change much in any of the four possible combinations, as do the other two variables representing the losses induced by impurities and management cost of the electrolyte. Therefore, it can be confirmed that the previous calculations are valid.

In the worst case, i.e., when calculations are performed with maxima of both constants, the price of replacing the electrolyte is equal to c_{EM} = 0.5 M€. Therefore, the maximum additional cost related to the electrolyte replacement will be equal to 0.12 €/kg, that is an acceptable cost considering the previously calculated levelized cost of hydrogen.

6. Conclusions

The study conducted in this thesis demonstrate the technical and economic viability of the green hydrogen production through Alkaline electrolysers from desalinated seawater. After finishing the detailed investigation of this thesis, the following conclusions are drawn:

- **Choice of the electrolyzer type**

The *AWEs* currently represent the best option for hydrogen production at sea as they are the least sensitive technology to impurities and are already used in nuclear submarines to produce oxygen. In addition, it is possible to produce the electrolyte directly on-site through the Chloralkali process, avoiding the risk of electrolyte handling during replacement.

On the other hand, *AEMs* and *SOEs* have been discarded as they have low *TRL* and there is not enough knowledge about them, as well as *PEMs* that are highly sensible to impurities despite also being used at sea for the same purposes as *AWEs*.

- **Techno-economic analysis of a commercial Alkaline electrolyser**

It reveals that the case study LCoH is 6.25 €/kg, a value slightly higher than the ones found in literature papers due to the still high cost of electricity from renewable sources, which significantly influences the operating costs of the compressor and electrolysis.

However, it is estimated that this cost may drop dramatically in the recent future due to the increased supply of renewables, technological innovation and energy efficiency in energy production and transport.

Even the costs related to the CAPEX of the electrolyzer, the stack replacement, and the compressor maintenance, which today account for a significant share of hydrogen production plant costs, are estimated to decrease steadily over time due to growing demand, technological innovation and the use of alternative materials that are cheaper and more efficient than the current ones.

- **Choice of the optimal number of series distillation**

Experimental analysis has shown that serial distillation only causes an increase in costs, without an increase in benefits. A single distillation is enough to achieve acceptable salinity levels to be used in the electrolyzer. However, even greater purity can be achieved by using other more efficient processes, such as electrodialysis, after the first distillation.

- **Selection of the suitable material for the cell 3D printing**

The second part of the laboratory experiments shows that it is possible to create a functional alkaline cell from polypropylene, and that *PLA* does not exhibit characteristics suitable for use in contact with caustic soda.

- **Evaluation of the electrolyte degradation trend**

Hydrogen production shows that the increasing presence of residual impurities in the electrolyte from desalinated seawater causes an increase in cell voltage and a consequent deterioration in electrolyser performance. For the first time in the available literature, electrolyte degradation presents a reasonably precise logarithmic trend, which makes it possible to calculate the renewal time of the electrolyte and its cost of management at sea.

- **Evaluation of the electrolyte renewal time and management costs**

The high-efficiency operation time of the electrolyte in the presence of desalinated saltwater is found to be one-fifth of the operating hours of the electrolyzer, a very interesting result that indicates that only five replacements are required in the entire life cycle of the electrolyzer.

Finally, the additional cost result shows that electrolysis from desalinated seawater is economically feasible because it represents only the 8% of the total system cost and a percentage lower than 2% with respect to the total levelized cost of hydrogen.

In conclusion, although these laboratory experiments yielded excellent results, further research and investigation is needed to improve seawater electrolysis and make this technology even more commercially competitive.

Annex A: Commercial electrolyzers database

Producer	Type	Model	H2 production [Nm3/h]	Power [kW]	Specific energy consumption [kWh/Nm3]	Dimension [m2]	Efficiency [%]	Water consumption [l/Nm3]	Outlet pressure [bar]
Cummins	AWE	Hystat-10	10	115	4.52	54	0.31	1.2-2	10
Cummins	AWE	Hystat-15	15	155	4.52	54	0.34	1.2-2	10
Cummins	AWE	Hystat-30	30	275	4.52	54	0.39	1.2-2	10
Cummins	AWE	Hystat-60	60	550	4.52	89	0.39	1.2-2	10
Cummins	AWE	Hystat-70	70	675	4.52	89	0.37	1.2-2	10
Cummins	AWE	Hystat-100	100	800	4.52	89	0.44	1.2-2	10
McPhy	AWE	McLyzer 100-30	100	500	4.5	n.d.	0.71	n.d.	30
McPhy	AWE	McLyzer 400-30	400	2,000	4.5	n.d.	0.71	n.d.	30
McPhy	AWE	McLyzer 800-30	800	4,000	4.5	n.d.	0.71	n.d.	30
Brise Chemicals	AWE	AE-5	5	23	4.1	125-2,000	0.77	n.d.	n.d.
Brise Chemicals	AWE	AE-300	300	23-1,680	4.1	125-2,000	n.d.	n.d.	n.d.
Brise Chemicals	AWE	AE-2000	2,000	23-1,680	4.1	125-2,000	n.d.	n.d.	n.d.
Sunfire	AWE	Hylink	2,165	10,000	4.35	375	0.77	0.81	30
Thyssenkrupp	AWE	n.d.	4,000	20,000	4.5	n.d.	0.79	n.d.	30
Nel	AWE	A150	150	n.d.	4.1	150	n.d.	n.d.	1-200
Nel	AWE	A1000	1,000	n.d.	4.1	225	n.d.	n.d.	1-200
Nel	AWE	A20000	20,000	n.d.	4.1	>770	n.d.	n.d.	1-200
Longi	AWE	LHy-A800	800	4,000	4.15	260	0.71	n.d.	16
Longi	AWE	LHy-A1000	1,000	5,000	4.15	260	0.71	n.d.	16
Longi	AWE	LHy-A1500	1,500	7,500	4.15	280	0.71	n.d.	16
Green Hydrogen Systems	AWE	HyProvide A 90	90	418	4.33	n.d.	0.76	0.9	35
John Cockerill	AWE	DQ1000	1,000	5,000	4.41	15.18	0.71	0.92	30
Enapter	AEM	EL 4.0	0.5	3	4.8	0.31	0.59	n.d.	35
H2B2	PEM	EL 0.5N	0.5	3.2	4.7	1.44	0.55	<1	1-20
H2B2	PEM	EL 10N	10.05	53.2	4.7	7.2	0.67	<1	15-40
H2B2	PEM	EL 100N	100	515	4.7	48	0.69	<1	15-40
H2B2	PEM	EL 800N	800	4,130	4.7	28.8	0.69	<1	15-40
ITM POWER	PEM	HGAS1SP	122.4	707	4.7	n.d.	n.d.	1.78	20
ITM POWER	PEM	HGAS3SP	278.1	2,070	n.d.	n.d.	n.d.	n.d.	30
ITM POWER	PEM	3MEP CUBE	400.4	2,000	n.d.	n.d.	n.d.	n.d.	30
Cummins	PEM	HyLYZER-1000	1,000	7,000	4.3	n.d.	0.51	0.9	30
Cummins	PEM	HyLYZER-500	500	3,200	4.3	198	0.55	1.2-1.5	30
Cummins	PEM	HyLYZER-250	250	1,700	4.3	198	0.52	1.2-1.5	30
Elogen	PEM	E5	5	40	5.7	n.d.	0.44	1.43	35
Elogen	PEM	E30	30	240	5.1	n.d.	0.44	1.28	35
Elogen	PEM	E120	120	960	4.8	n.d.	0.44	1.2	35
H-TEC	PEM	ME450	210	1,000	4.7	52.8	0,75	n.b.	20-30
H-TEC	PEM	HCS	2,100	10,000	4.7	18.36	0,75	1.39	20-30
Bloom Energy	PEM	n.d.	2,522	10,000	4.14	n.d.	n.d.	n.d.	30
Plug	PEM	EX-425D	200	1,000	4.49	29.3	0.71	1.03	40
Plug	PEM	EX-4250D	2,000	10,000	4.49	117.2	0.71	1.03	40
Siemens	PEM	Silyzer 300	22,247	70,000	n.d.	1,750	0.75	n.d.	n.d.
Proton	PEM	M200	200	1,000	n.d.	n.d.	n.d.	n.d.	30
Proton	PEM	M400	400	2,000	n.d.	n.d.	n.d.	n.d.	30
Sunfire	SOE	Hylink HL40	40	150	3.7	n.d.	0.82	n.d.	10
Sunfire	SOE	Hylink HL200	200	750	3.7	n.d.	0.82	n.d.	n.d.

Table 32: Commercial water electrolyzers

The table above provides an overview of some of the electrolyzers currently on the market, with data taken from the data sheets on each manufacturer's website. The table indicates with n.d. any data omitted from the data sheet, and in red all values that have been calculated from the data provided.

Annex B: Problems and inconveniences

- Distillation

The first attempt to find the rejection rate is made through the distillation of various one-liter solutions of distilled water to which different amounts of the same salt had previously been added. Each experiment involves doubling the amount of salt in the solution of the previous experiment. More specifically, the first experiment is conducted by inserting only 1 gram of salt, the second with 2 grams, and so on, always doubling the value until reaching 8 grams.

Initially, pre-, and post-distillation salinity are measured with a salt meter, which give us in output an amount in parts per million [ppm]. However, the measurements are discarded due to some inaccuracies of the instrument. To obtain more precise measurements, it is decided to change the measuring device and use a conductivity meter to investigate whether a mathematical relationship could be derived between solution conductivity and rejection rate.

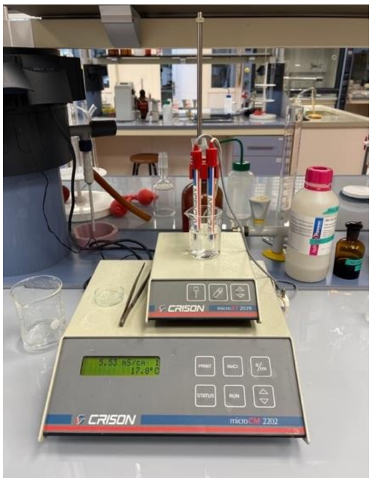

Figure 53: Conductivity meter in the UPM chemistry laboratory

The distillation process of the solutions is then repeated, and these results are obtained:

	Before [ppm]	Before [mS/cm]	After [ppm]	After [mS/cm]
1g NaCl	718	1.31	Out of the range	3.94E-03
2g NaCl	1760	3.09	Out of the range	3.59E-03
4g NaCl	3320	5.53	Out of the range	2.78E-03
8g NaCl	6130	9.87	Out of the range	3.40E-03

Table 33: Results related to ppm and conductivity before and after the distillation

This second attempt is useful to understand the relationship between salinity and conductivity before the distillation process but does not provide the expected post-distillation results.

In Figure 54 it is possible can see the linear increasing trend in the conductivity of a solution as its salinity increases. This occurs because the ionized salts in the solution can conduct electric current, so the more salts there are in the solution, the higher its conductivity will be.

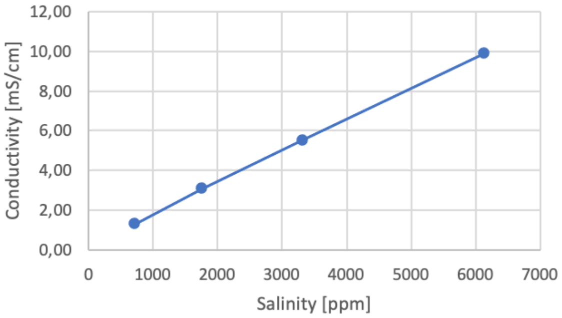

Figure 54: Conductivity evolution with respect to salinity

From the post-distillation measurements, a higher salt presence is expected in the solutions with higher initial salt concentration. However, as can be seen in Table 33 for NaCl measurements, similar and approximately constant values of conductivity are obtained in all measurements and values outside the range of salinity measurements.

From a certain point of view, these data are positive since they indicate to us that the presence of salt remaining after distillation is very low and therefore the electrolyte can last longer. On the other hand, they do not allow us to find a mathematical equation that would allow to understand the variation in rejection rate as salinity changes.

It is also carried out a third attempt increasing the differences in salt concentrations between solutions to verify that the error is not using too small salt variations. Again, inaccurate results are obtained because the amounts of salt present in the post-distillation remain very low.

- Hydrogen production

Although it is known that the most suitable material is polypropylene, as it has a higher melting point and greater chemical resistance, the first printing is done with PLA.

The cell is assembled and then connected to the *Heidolph Pumpdrive 5201* peristaltic pump through tubes made of polypropylene initially circulating only water at the operating temperature from the thermostatic bath. After checking the temperature resistance of the cell at a temperature of 60°C, the electrolyte is prepared.

By running caustic soda inside the cell, it is shown that this material is unsuitable even for conducting short experiments because within minutes as can be seen in Figure 55, cracks form in the different layers and one of the outlet tubes collapses.

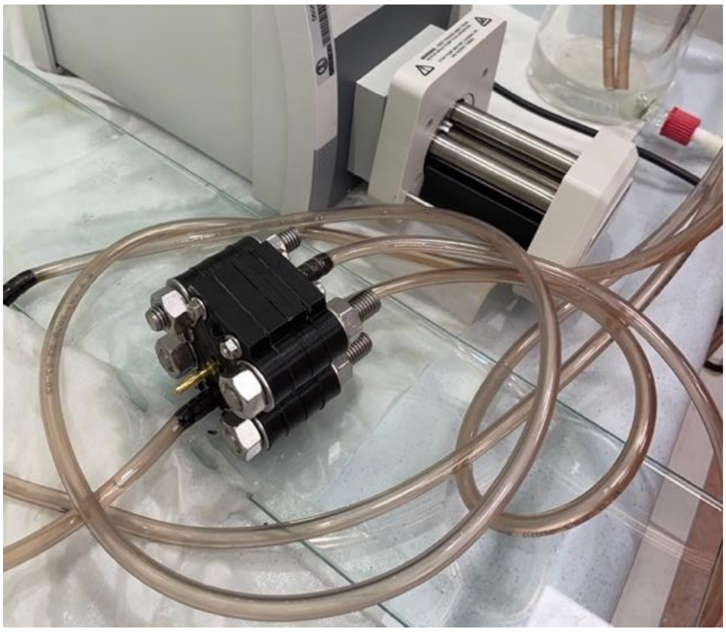

Figure 55: PLA cell collapse due to low resistance to chemicals

Acknowledgements

First, I would like to thank Prof. d'Amore-Domenech, the supervisor of this thesis, for the continuous support he has given me throughout the entire drafting period and for all the scientific notions he has taught me with great passion, availability, and patience. Next, I would like to thank Prof. Lanzini for having believed in this project from the first moment I proposed it to him and for having given me the opportunity to write my thesis abroad at a prestigious university such as the Universidad Politécnica de Madrid, acting as my internal supervisor.

A big thank you goes to my entire family, who always believed in me and supported me in every choice I made. In a special way, I thank my parents for giving me the opportunity to study in Italy and abroad without ever missing anything and for being by my side even in the most difficult moments of my university career. To my mother, the first person to rejoice at my victories and the first to console me and lift me up after defeats, and to my father, who constantly kept my feet on the ground and always pushed me to give my best and never give up.

Special thanks go to my best friend *Josemi*, a true irreplaceable brother that I can no longer do without. Thank you for being the shoulder I can rely on every day, for being a sincere friend I can trust blindly and who always manages to bring out the best in me. I am truly grateful to have known you and I would really like to thank you for all the time you have given me over the years, for patiently putting up with even the worst parts of my character by always being by my side and above all for welcoming me into your home and making me feel at home even thousands of kilometers away.

To *Carlos, Delfi* and *Paco*, my Spanish family. Thank you for all the affection and love you have shown me since the first day I met you, because it is thanks to you that I feel at home in Madrid. Thank you for the wonderful welcome, for all the lunches and dinners you have prepared for me with love, spoiling me as if I were your own son. This is only done by people with a huge heart, like you.

My thanks also go to my lifelong Sicilian friends who have been by my side throughout this journey and who make me feel as if I had never left when I return to Sicily. I would also like to thank *Erika* who has always been able to advise me in the best way possible

and who has been by my side even in the most difficult moments of this journey, patiently listening to all my misfortunes via video call.

To the guys of the Valladolid *"Salottino"* who made me live the best experience of my life and who showed me that Erasmus is not, as you think, just party and fun, but also a unique chance to create real relationships. A special thanks to *Ste* who proved to be a real brother, capable of understanding me thoroughly and motivating me to overcome all my limits.

Last but not least, I must thank all the guys with whom I shared this unforgettable university journey in Turin who made achieving this goal easier and more fun. Thank you for every moment spent together, for all the trips and experiences that have allowed us to bond more and more, and for helping me through difficult times, especially in the first years of university. Special mention for *Simo, Ema, Lorenzo* as well as my housemates, *Cosp, Baru, Vez* and *Paolo*.

To *Cosp*, for whom I have infinite respect and who understood everything from the start. Thank you for that message of encouragement you sent me at the worst time of my journey, know that it was too important for me. Thank you for believing in me from moment zero, I will always be grateful.

References

Abdel-Aal H.K., Z. K. (2010). Hydrogen Production Using Sea Water Electrolysis. *The Open Fuel Cells Journal*.

Al-Amshawee S., Y. B. (2020, January 15). Electrodialysis desalination for water and wastewater: A review. *Elsevier*.

Al-Obaidi M.A., Z. R.-A. (2022, September 8). energies. *Evaluation of Solar Energy Powered Seawater Desalination Processes: A Review.*

Arias L.A., R. E. (2018). A Review and Analysis of Trends Related to Demand Response. *Energies*.

Barelli L., B. G. (2017, November). Airflow Management in Solid Oxide Electrolyzer(SOE) Operation: Performance Analysis. *Chemengineering*.

Bocanegra-Bernal M.H., D. d. (2002). Phase transitions in zirconium dioxide and related materials for high performance engineering ceramics. *Journal of Materials Science*.

Brauns J., T. T. (2020, February 21). Alkaline Water Electrolysis Powered by Renewable Energy: A Review. *Processes*.

Brisse A., S. J. (2008). High temperature water electrolysis in solide oxide cells. *International Journal of Hydrogen Energy*.

Britannica, T. E. (2022, May 12). *sodium hydroxide*.

Buttler A., S. H. (2018). Current status of water electrolysis for energy storage, grid balancing and sector coupling via power-to-gas and power-to-liquids: A review. *Elsevier*.

Carmo M., F. D. (2013). A comprehensive review on PEM water electrolysis. *Elsevier*.

Chapter 9 - Electrochemical hydrogen generation. (2019). In M. K. Ali Keçabas, *Solar hydrogen production* (pp. 299-317).

Chen K., A. N. (2010). Development of (Gd , Ce) O2-Impregnated (La , Sr) MnO3 Anodes of High Temperature Solid Oxide Electrolysis Cells. *Journal of The Electrochemical Society, Volume 157, Number 11*.

Chi J, Y. H. (2018). Water electrolysis based on renewable energy for hydrogen production. *Elsevier*.

Curto D., F. V. (2021, January 12). A Review of the Water Desalination Technologies. *applied sciences*.

D'Amore-Domenech R., S. O. (2020, August 2). Multicriteria analysis of seawater electrolysis technologies for green hydrogen production at sea. *Elsevier*.

D'Amore-Domenech, R. (2021). Study on the production of hydrogen through the electrolysis of seawater in a sustainable marine context.

Do Thi H.T., P. T. (2021). Comparison of Desalination Technologies Using Renewable Energy Sources with Life Cycle, PESTLE, and Multi-Criteria Decision Analyses. *Water*.

Doornbusch G.J., T. M. (2019, August 15). Experimental investigation of multistage electrodialysis for seawater desalination. *Elsevier*.

Du F., W. D. (2018). Sodium Hydroxide Production from Seawater Desalination Brine: Process Design and Energy Efficiency. *Environmental Science & Technology*.

Elberry A.M., T. J.-A. (2021, April 26). Large-scale compressed hydrogen storage as part of renewable electricity storage systems. *Elsevier*.

Elga Veolia. (2021, September 9).

Elga Veolia. (2021, September 9). *Reverse Osmosis*.

Elsaid K., K. M. (2020, December 15). Environmental impact of desalination technologies: A review. *Sceince of The Total Environment*.

envaselia. (n.d.). *Qué es el polipropileno*.

Euronews. (2020). *euronews.green*.

Fasano M., M. M. (2020).

Felfil. (n.d.).

Fuel Cell Store. (2023). *Chlor-alkali Production Membranes*.

Gorre J., R. F. (2020). Cost benefits of optimizing hydrogen storage and methanation capacities for Power-to-Gas plants in dynamic operation. *Elsevier: Applied Energy*.

Gorre J., R. F. (2020). Cost benefits of optimizing hydrogen storage and methanation capacities for Power-to-Gas plants in dynamic operation. *Elsevier*.

Hatchbox. (n.d.). *What is 3D printer resin?*

Head, D. &. (n.d.). Multi Stage Flash (MSF). Mumbai.

IEA. (2021, Luglio). *Emissioni Nette pari a Zero entro il 2050, Una Tabella di Marica per il Settore Energetico Globale.*

IEA. (2023). *Electrolysers*.

International PtX Hub. (2023). *Water electrolysis explained – the basis for most Power-to-X processes*.

IRENA. (2021). *Renewable Power Generation Costs in 2021.*

IRENA. (2022). *International Renewable Energy Agency.*

IRENA. (2022). *Renewable Power Remains Cost-Competitive amid Fossil Fuel Crisis* .

ITWReagents. (n.d.). *PanReac AppliChem*.

Jun Chi, H. Y. (2018, March 5). Water electrolysis based on renewable energy for hydrogen production. *Science Direct*.

Khawaji A.D., K. I. (2008). Advances in seawater desalination technologies. *Elsevier*.

KREAfil. (n.d.).

La Gazzetta dello Sport. (2023). *sicurauto.it*.

letslab. (n.d.). *Vai all'inizio della galleria di immagini Idrossido di sodio in pastiglie AGR 1-2 mm Ph.Eur.*

Lucia, U. (2014). Overview on fuel cells. *Renewable and Sustainable Energy Reviews.*

López-Fernández E., G. S.-R.-E.-C. (2021, October 20). Recent Advances in Alkaline Exchange Membrane Water Electrolysis and Electrode Manufacturing. *molecules.*

M., P. (1990). *Handbook of Industrial Membrane Technology.* Noyes Publications.

MatterHackers. (n.d.).

Medicine, N. L. (2023). *National Center for Biotechnology Information.*

Meng, N. (2006). An Overview of Hydrogen Storage Technologies. *Energy exploration & exploitation.*

Mezher T., F. H. (2011). Techno-economic assessment and environmental impacts of desalination technologies. *Elsevier.*

Miller H.A., B. K.-H. (2020). Green hydrogen from anion exchange membrane water electrolysis: a review of recent developments in critical materials and operating conditions. *Sustainable Energy Fuels.*

Millero F.J., F. R. (2007, October 7). The composition of Standard Seawater and the definition of the Reference-Composition Salinity Scale. *Elsevier.*

Mohammadifakhr M., d. G. (2020). Forward Osmosis: A Critical Review. *processes.*

natives, 3. (2022, June 6). *All You Need to Know About PVA for 3D Printing* .

Nechache A., H. S. (2021). Alternative and innovative solid oxide electrolysis cell materials: A short review. *Renewable and Sustainable Energy Reviews.*

NetSol Water. (2022). *What is Electrodialysis and its advantages?*

Nguyen T., A. Z. (2019). Grid-connected hydrogen production via large-scale water electrolysis. *Elsevier.*

Ni M., L. M. (2008). Technological development of hydrogen production by solid oxide electrolyzer cell (SOEC). *Elsevier.*

Nikolay, V. (2013). *Desalination Engineering: Planning and Design.* The McGraw-Hill Companies.

Osman A.I., M. N.-H.-M. (2021, October 6). Hydrogen production, storage, utilisation and environmental impacts: a review. *Environmental Chemistry Letters.*

Peterson D., M. E. (2016). Hydrogen production cost from solid oxide electrolysis. *Hydrogen and fuel cells program record.*

Protank. (2023). *Sodium Hydroxyde Storage Tanks & Specifications.*

Rashid M.M., A. M. (2015, February). Hydrogen Production by Water Electrolysis: A Review of Alkaline Water Electrolysis, PEM Water Electrolysis and High Temperature Water Electrolysis. *International Journal of Engineering and Advanced Technology.*

Richardson I., F. J. (2015). *Low-cost, Transportable Hydrogen Fueling Station for Early FCEV Adoption.*

Rodríguez J., A. E. (2020, December 11). CFD Modeling and Experimental Validation of an Alkaline Water Electrolysis Cell for Hydrogen Production. *processes*.

Ruth M., M. A. (2017, August 11). Manufacturing Competitiveness Analysis for PEM and Alkaline Water Electrolysis Systems.

Saadat A.H.M., I. M. (2018, January). Desalination Technologies for Developing Countries: A Review. *Journal of Scientific Research*.

Shiva Kumar S., L. H. (2022, July 21). An overview of water electrolysis technologies for green hydrogen production. *Elsevier*.

Shreve R.N., B. J. (1977). In *Chemical Process Industries* (p. 219).

Sood S., P. O.-B. (2020). Generic Dynamical Model of PEM Electrolyser under Intermittent Sources. *Energies*.

Sorbi, M. (2022, June 30). *ilGiornale.it*.

STAMPA3Dstore.com. (n.d.). *La stampante 3D DLP Inkspire, Zortrax entra nel mercato della stampa 3D in resina.*

Tan S.Y., C. V.-O. (2020). Teaching the Nernst Equation and Faradaic Current through the Use of a Designette: An Opportunity to Strengthen Key Electrochemical Concepts and Clarify Misconceptions. *Journal of Chemical Education*.

Treccani. (2023). *Elettrolisi*.

United Nations Climate Change. (2023). *The Paris Agreement*.

Vedantu. (n.d.). *Reverse Osmosis*.

Veolia. (n.d.). *Multiple Effect Distillation (MED)* .

Voldsund M., J. K. (2016). Hydrogen production with CO2 capture. *Elsevier*.

VOW. (2023). *Biogreen a part of VOW*.

Wade M. (2000). Distillation plant development and cost update. *Elsevier*.

Wang J., H. E. (2022, June 20). Opportunities and Challenges of Seawater Desalination Technology. *frontiers*.

Wang W., W. X. (2015). Electrochemical cells for medium- and large-scale energy storage: fundamentals. *Elsevier*.

Wang Y., L. W. (2020, October). Degradation of Solid Oxide Electrolysis Cells: Phenomena, Mechanisms, and Emerging Mitigation Strategies – A Review. *Journal of Materials Science and Technology*.

Wang Y., Y. H. (2021). Polymer electrolyte membrane fuel cell and hydrogen station networks for automobiles: Status, technology, and perspectives. *Elsevier*.

Wang, D. L. (2022). Direct Electrolytic Splitting of Seawater: Significance and Challenges. *Coatings*, 3.

Yue X., Y. A. (2008). Investigation on scandium-doped manganate $La_{0.8}Sr_{0.2}Mn_{1-x}Sc_xO_{3-\delta}$ cathode for intermediate temperaturesolid oxide fuel cells. *Journal of Power Sources*.

Zhang F., Z. P. (2016). The survey of key technologies in hydrogen energy storage. *Elsevier*.

Zhang X., S. Y. (2017, September). Co-electrolysis of CO_2 and H_2O in high-temperature solid oxide electrolysis cells: Recent advance in cathodes. *Journal of Energy Chemistry*.